AGU PUBLICATIONS

JGR

Journal of Geophysical Research: Earth Surface

RESEARCH ARTICLE
10.1002/2015JF003620

Key Points:
- Waterfall plunge pools are dynamic and transient repositories for sediment
- Plunge pools self-adjust their depth to pass the upstream sediment load
- Sediment-transport capacity increases for larger waterfalls and shallower pools

Supporting Information:
- Supporting Information S1
- Table S1
- Table S2
- Movie S1
- Codes S1

Correspondence to:
J. S. Scheingross,
joel.scheingross@gfz-potsdam.de

Citation:
Scheingross, J. S., and M. P. Lamb (2016), Sediment transport through self-adjusting, bedrock-walled waterfall plunge pools, *J. Geophys. Res. Earth Surf.*, *121*, 939–963, doi:10.1002/2015JF003620.

Received 26 MAY 2015
Accepted 11 MAR 2016
Published online 13 MAY 2016

Sediment transport through self-adjusting, bedrock-walled waterfall plunge pools

Joel S. Scheingross[1,2] and Michael P. Lamb[1]

[1]Division of Geological and Planetary Sciences, California Institute of Technology, Pasadena, California, USA, [2]Now at Helmholtz Centre Potsdam German Research Center for Geosciences (GFZ), Potsdam, Germany

Abstract Many waterfalls have deep plunge pools that are often partially or fully filled with sediment. Sediment fill may control plunge-pool bedrock erosion rates, partially determine habitat availability for aquatic organisms, and affect sediment routing and debris flow initiation. Currently, there exists no mechanistic model to describe sediment transport through waterfall plunge pools. Here we develop an analytical model to predict steady-state plunge-pool depth and sediment-transport capacity by combining existing jet theory with sediment transport mechanics. Our model predicts plunge-pool sediment-transport capacity increases with increasing river discharge, flow velocity, and waterfall drop height and decreases with increasing plunge-pool depth, radius, and grain size. We tested the model using flume experiments under varying waterfall and plunge-pool geometries, flow hydraulics, and sediment size. The model and experiments show that through morphodynamic feedbacks, plunge pools aggrade to reach shallower equilibrium pool depths in response to increases in imposed sediment supply. Our theory for steady-state pool depth matches the experiments with an R^2 value of 0.8, with discrepancies likely due to model simplifications of the hydraulics and sediment transport. Analysis of 75 waterfalls suggests that the water depths in natural plunge pools are strongly influenced by upstream sediment supply, and our model provides a mass-conserving framework to predict sediment and water storage in waterfall plunge pools for sediment routing, habitat assessment, and bedrock erosion modeling.

1. Introduction

Landscape evolution in mountain areas is often set by waterfall processes, where waterfalls can retreat at rapid rates and determine landscape response to changes in climate and tectonics [e.g., *Crosby and Whipple*, 2006; *Mackey et al.*, 2014; *DiBiase et al.*, 2015]. Many waterfalls have deep, bedrock plunge pools at their base (e.g., Figure 1). Such pools have been argued to focus bedrock erosion through undercutting of the waterfall face [e.g., *Gilbert*, 1890, 1907; *Holland and Pickup*, 1976; *Haviv et al.*, 2010] and vertical incision at the plunge pool floor [*Howard et al.*, 1994; *Lamb et al.*, 2007], although additional waterfall erosion mechanisms exist including toppling of bedrock columns [e.g., *Young*, 1985; *Weissel and Seidl*, 1997; *Lamb and Dietrich*, 2009].

Over annual timescales waterfall plunge pools can fill with sediment and evacuate to intermittently expose the bedrock pool floor (Figures 1a–1d). Plunge pools that are empty or partially filled with sediment provide critical habitat for a wide range of aquatic organisms [e.g., *Hawkins et al.*, 1993]. Low water velocities within plunge pools may provide refuge for aquatic organisms during periods of high flow [e.g., *Rempel et al.*, 1999]. During warm periods, thermal stratification of deep pools provides cool water, allowing fish to escape lethal surface temperatures [*Matthews et al.*, 1994; *Nielsen et al.*, 1994; *Torgersen et al.*, 1999]. During droughts, individual plunge pools can provide isolated refugia for invertebrates and fish [*Boulton*, 2003; *Lake*, 2003; *Magoulick and Kobza*, 2003] and have been highlighted as areas of high priority for protection from disturbance and sedimentation [*Bond et al.*, 2008]. These ecological benefits are diminished when plunge pools completely or near-completely fill with sediment, and instead, filled pools in steep mountain catchments pose a natural hazard, as the availability of a thick, alluvial deposit below a waterfall jet provides ideal conditions to mobilize debris flows [e.g., *Griffiths et al.*, 2004; *Larsen et al.*, 2006; *Godt and Coe*, 2007]. As such, developing plunge-pool sediment-transport capacity theory can aid land managers to predict habitat availability and assess natural hazards.

Despite progress in predicting sediment transport in steep streams [e.g., *Yager et al.*, 2007; *Recking*, 2009; *Nitsche et al.*, 2011; *Prancevic et al.*, 2014], including streams with small vertical steps [*Zimmermann et al.*, 2010; *Yager et al.*, 2012], it is difficult to apply existing models to waterfall plunge pools, where the impinging waterfall jet and deep plunge pool create significantly different hydraulics than those assumed in existing

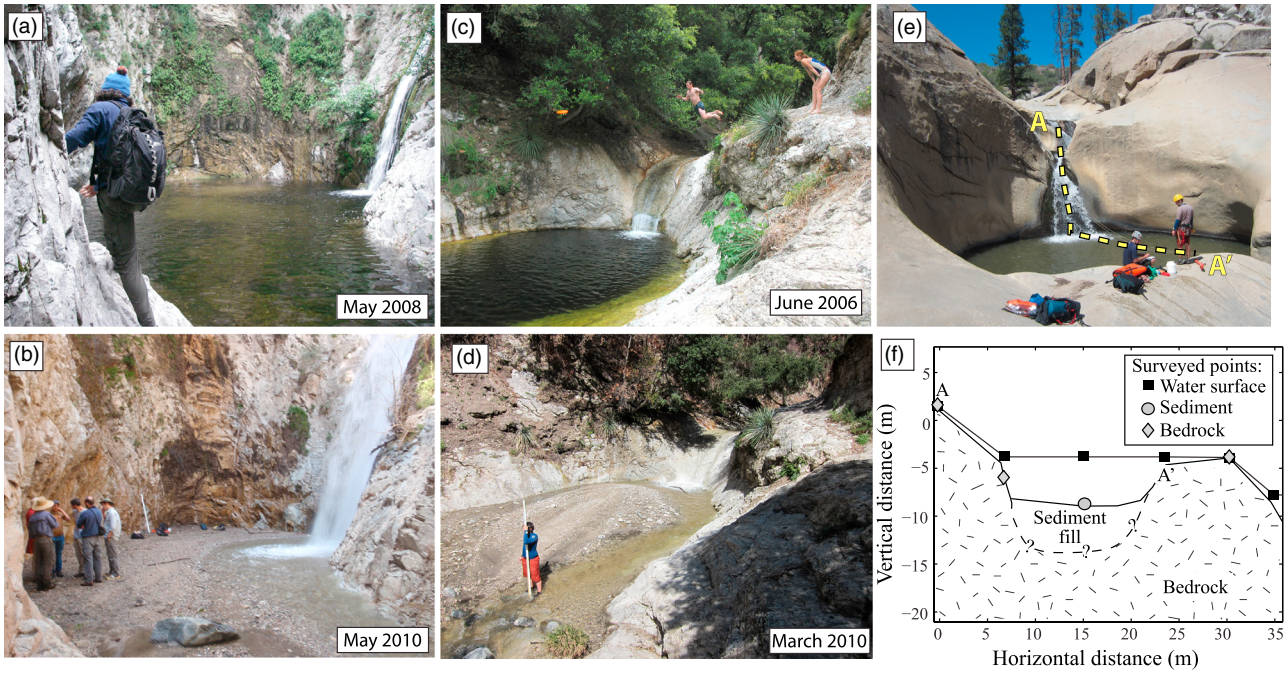

Figure 1. Figures 1a–1d are examples of sediment filling and evacuation of waterfall plunge pools on Arroyo Seco, San Gabriel Mountains, California. (a and b) Upper Switzer Falls (USF, Table S1); (c and d) an unnamed ~2.5 m bedrock step (ASP4, Table S1). (e) Photo and (f) surveyed long-profile through a deep waterfall plunge pool with cylindrical geometry on Dry Meadow Creek, California (STC3, Table S1).

sediment transport models designed for channelized flow [e.g., *Meyer-Peter and Mueller*, 1948]. Over long timescales, plunge-pool sediment-transport capacity is a key unknown needed to make more realistic waterfall retreat models [*Lamb et al.*, 2007, 2015], and the lack of a specific theory has led to the application of river erosion models to waterfalls [e.g., *Chatanantavet and Parker*, 2006; *Berlin and Anderson*, 2007; *Crosby et al.*, 2007], which may be inappropriate.

Most existing work on sediment transport through plunge pools has focused on soil-mantled landscapes where plunge pools form beneath small alluvial headcuts, and below man-made dams and sills. For example, *Mason and Arumugam* [1985] compiled laboratory and larger-scale prototype data from engineered overfalls and spillways to develop an empirical formula predicting plunge-pool scour depth under clear-water discharge. Field studies [*Lenzi and Comiti*, 2003; *Lenzi et al.*, 2003] and laboratory experiments [*Lenzi et al.*, 2002; *Gaudio and Marion*, 2003; *Marion et al.*, 2004; *Tregnaghi et al.*, 2011] have led to empirical relationships to predict steady-state geometry and time evolution of scour holes formed beneath sills and check dams. Similarly, Pagliara and colleagues have conducted laboratory experiments on various aspects of plunge pools formed in loose sediment [e.g., *Pagliara et al.*, 2008a, 2010, 2012b]. *Stein et al.* [1993] employ an approach which has been widely adopted [e.g., *Alonso et al.*, 2002; *Hanson et al.*, 2002; *Flores-Cervantes et al.*, 2006] to predict the equilibrium plunge-pool depth in loose sediment based on the threshold of grain motion.

Applying the existing work to bedrock-walled plunge pools in mountain streams is difficult for two main reasons. First, existing work has focused on plunge pools developed in loose sediment where the plunge-pool geometry evolves over similar timescales as changes in flow hydraulics [e.g., *Stein and Julien*, 1993; *Gaudio and Marion*, 2003; *Pagliara et al.*, 2008b] and sediment supply [e.g., *Marion et al.*, 2006; *Wells et al.*, 2010; *Pagliara et al.*, 2011, 2012a]. This is in contrast to bedrock-walled plunge pools (e.g., Figure 1), where the bedrock geometry likely evolves over order 10^2–10^5 year timescales, such that the flow hydraulics and bedrock geometry are decoupled over individual floods. Sediment fill, however, can be deposited on top of the bedrock pool floor, allowing water depths to vary in response to changing hydraulics and sediment supply over individual flood timescales (e.g., Figure 1).

Second, for plunge pools below channel headcuts and dams, there is often negligible sediment supply from upstream, thereby enhancing the ability of the waterfall jet to scour loose sediment from the plunge pool

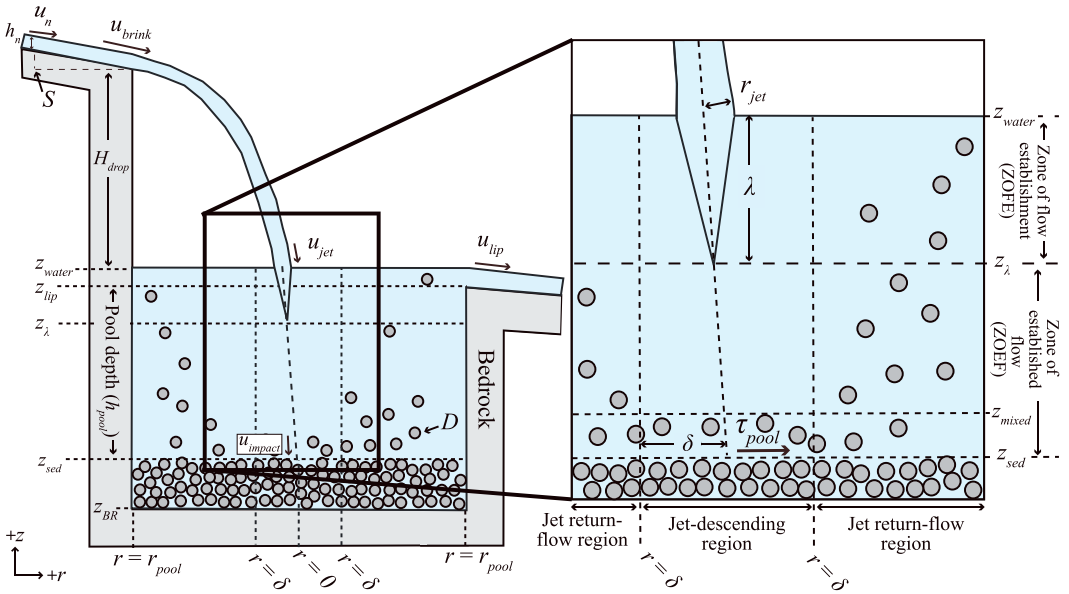

Figure 2. Schematic of waterfall plunge pool system with key variables labeled (modeled after *Flores-Cervantes et al.* [2006]). Inset shows jet-descending and return-flow regions, as well as zones of flow establishment (ZOFE) and established flow (ZOEF). Variables: h_n = normal flow depth upstream of waterfall, h_{pool} = plunge-pool depth, H_{drop} = waterfall drop height, S = channel slope, r_{jet} = waterfall jet radius at impact with plunge-pool water surface, r_{pool} = plunge-pool radius, u_{brink} = water velocity at waterfall brink, u_{jet} = waterfall jet velocity at impact with plunge-pool water surface, u_{lip} = water velocity at downstream plunge-pool lip, u_n = normal flow velocity upstream of the waterfall, z_{BR} = elevation of plunge-pool bedrock floor, z_{lip} = elevation of downstream plunge-pool lip, z_{mixed} = elevation of the top of the well-mixed layer near the pool floor, z_{sed} = elevation of plunge-pool alluvial floor, z_{water} = elevation of plunge-pool water surface, z_λ = elevation of transition between ZOEF and ZOFE, δ = radius of jet-descending region, λ = length of ZOFE, and τ_{pool} = plunge-pool bed shear stress.

compared to a natural river transporting sediment. Despite many studies on plunge-pool hydraulics [e.g., *Robinson et al.*, 2000; *Bennett and Alonso*, 2005; *Pasternack et al.*, 2007] and sediment transport under clear-water flow [e.g., *Bennett et al.*, 2000; *Lenzi et al.*, 2002; *Pagliara et al.*, 2006], there exist a limited number of experiments addressing the influence of upstream sediment supply on resulting plunge-pool depth [*Marion et al.*, 2006; *Wells et al.*, 2010; *Pagliara et al.*, 2011, 2012a]. These experimental studies show that through sediment deposition, plunge pools tend to shallow their depths in response to increasing sediment supply when all else is held constant; however, no theory has been developed to date to predict equilibrium pool depth as a function of sediment supply.

In this paper we focus on sediment transport mechanics in deep waterfall plunge pools which have steep bedrock sidewalls and sediment deposited over bedrock floors (e.g., Figure 1). We first propose a conceptual model where plunge-pool sediment-transport capacity is modulated by dynamic adjustment of pool depth. Herein the term pool depth refers to the vertical distance bounded by the downstream plunge-pool lip and the top of the alluvial fill (if it exists) at the pool floor (Figure 2) and represents the depth of water in the pool at the condition of vanishing overflow into the downstream river reach (e.g., the residual pool depth in the sense of *Lisle* [1987] and *Lisle and Hilton* [1992]). The pool floor can be sediment or bedrock, but in this paper we refer only to adjustment of the alluvial floor. Second, we develop a physically based model to predict the sediment-transport capacity and equilibrium pool depth of bedrock-walled waterfall plunge pools. Third, we describe controlled laboratory experiments designed to test the model and explore model predictions. Finally, we discuss limitations of the model, application to field scale, and the implication of these results in the context of plunge-pool sediment transport over short timescales, and bedrock erosion over longer timescales.

2. Hypothesis and Motivation

Similar to alluvial rivers which self-adjust their slope, width, and depth in response to changes in sediment supply and water discharge [e.g., *Mackin*, 1948; *Lane*, 1955], we hypothesize that bedrock-walled waterfall plunge pools are dynamic systems that self-adjust their depth through erosion and deposition of sediment

to maintain an equilibrium between plunge-pool sediment-transport capacity (Q_{sc_pool}, units of [L^3/T], see the notation section) and the imposed sediment supply from upstream (Figure 2). Thus, at equilibrium conditions, the sediment flux into the pool equals the sediment flux out, and the pool depth is at a steady state as long as the underlying bedrock floor is not exposed. For example, we expect the equilibrium pool depth for a given sediment supply and water discharge to transiently aggrade following an increase in sediment supply or decrease in water discharge. In turn, as the pool shallows, we expect an increase in the capacity of the jet to transport sediment out of the pool, thus decreasing the imbalance between sediment supply and transport capacity, and leading eventually to a new, shallower steady-state depth. The same negative feedback should hold following a decrease in sediment supply or increase in water discharge, whereby pools are expected to transiently scour and deepen until either a new, deeper equilibrium depth is reached or the bedrock floor is exposed.

Changes in plunge-pool depth influence Q_{sc_pool} in at least two distinct ways. First, greater pool depths result in a reduction in bed shear stress at the pool floor, as the waterfall jet must diffuse through a deeper water column before impinging upon the bed, thus decreasing the ability of the jet to entrain sediment [e.g., *Albertson et al*., 1950; *Rajaratnam*, 1976; *Stein et al*., 1993]. Second, as pools deepen, sediment must be suspended higher in the water column in order to be transported over the plunge-pool walls and into the river reach downstream. Changes in pool depth might also influence lift forces within the pool [*Fiorotto and Rinaldo*, 1992; *Pasternack et al*., 2007], although this effect has yet to be studied in detail. Under this framework, the presence of upstream sediment supply in natural plunge pools should lead to shallower pool depths at equilibrium, all else held constant, compared to what is expected from clear-water overspill below dams and sills.

Our hypothesis of dynamic adjustment of pool depth in response to changes in sediment supply is consistent with field observations of sediment deposited over bedrock plunge-pool floors as well as cycles of sediment fill and evacuation in response to floods and fires (e.g., Figure 1). Quantitative predictions of sediment fill and evacuation require theory to predict waterfall plunge-pool sediment-transport capacity, which we develop below.

3. Theory

We seek to develop theory predicting waterfall plunge-pool sediment-transport capacity for pools with fixed, vertical bedrock walls and fluctuating levels of alluvial fill. Following our conceptual model above, plunge-pool sediment-transport capacity theory should also be capable of predicting equilibrium plunge-pool depth by iteratively solving for the pool depth at which sediment-transport capacity is equal to the imposed sediment supply. The ideal theory should not only work over short timescales (i.e., individual floods) when hydrodynamics and sediment transport are coupled in order to predict equilibrium pool depth but should also be computationally tractable to use over geomorphic timescales where plunge-pool bedrock geometry evolves due to abrasion from impacting particles [e.g., *Lamb et al*., 2007]. This approach is akin to a geomorphic transport law (in the sense of *Dietrich et al*. [2003]) and allows coupling with existing sediment transport and bedrock erosion models to include waterfall processes in larger-scale river long-profile and landscape evolution models.

Water flow in natural plunge pools exhibits complex velocity patterns where the impinging waterfall jet spreads within the pool before impacting the bed and circulating [e.g., *Robinson et al*., 2000; *Bennett and Alonso*, 2005; *Pasternack et al*., 2007]. Modeling flow fields requires running computationally intensive 3-D numerical simulations [e.g., *Xu et al*., 2002], which goes against our goal of developing theory which can be applied easily over long timescales. Instead, we make simplifying assumptions for the plunge-pool geometry and hydrodynamics to develop an analytical solution. Our model is simplified to cylindrical, bedrock-walled plunge pools and predicts transient deposition or scour of a planar alluvial fill deposited over a bedrock plunge-pool floor to reach a new, equilibrium depth (e.g., Figures 1f and 2). Following advances in river sediment-transport capacity, we develop a 1-D sediment-transport capacity theory for bedrock plunge pools under assumptions of a channel-spanning pool, a circular waterfall jet which impacts the center of the plunge-pool floor, and axisymmetric flow. We hypothesize that sediment transport is most sensitive to upward directed flow, which aids transport of grains up and out of pools. To this end, we simplify water flow within the plunge pool by assuming the pool can be divided into two separate regions, a cylindrical jet-descending region where the waterfall jet flows downward to the plunge-pool floor and entrains sediment, and an annular jet return-flow region where upward directed flow carries sediment to

the water surface and out of the pool (Figure 2). We neglect radial advection of sediment between the two regions and instead drive radial sediment transport by turbulent diffusion.

We describe plunge-pool hydraulics and sediment transport within a radial coordinate system with an origin at the point of jet impact on the plunge-pool floor where the vertical (z) and radial (r) coordinates are positive in the upward and outward direction, respectively (Figure 2). As shown in Figure 2, pool depth is defined as $h_{pool} = z_{lip} - z_{sed}$, where z_{lip} is the elevation of the downstream plunge-pool lip and z_{sed} is the elevation of the top of the sediment bed at the base of the pool. If the pool is evacuated to bedrock, then z_{sed} should be replaced with the elevation of the bedrock pool floor. Note that defining the upper limit of the pool depth to be z_{lip} rather than the elevation of the water surface ensures that pool depth is not a function of water stage, and therefore, dry pools can be compared to wet pools [*Lisle*, 1987]. A MATLAB script to calculate plunge-pool sediment-transport capacity based on the theory is included in the supporting information.

3.1. Plunge-Pool Bed Shear Stress

Existing river and jet hydrodynamic theories show that water accelerates toward the brink of the waterfall due to the loss of hydrostatic pressure [*Rouse*, 1936, 1937b; *Hager*, 1983], and, once past the brink, the waterfall jet is commonly modeled as accelerating during freefall through the air [e.g., *Stein et al*., 1993; *Ervine et al*., 1997]. After impacting the water surface of the plunge pool, the jet first travels a finite length before friction from the surrounding water is felt at the jet centerline; this zone is commonly referred to as the Zone of Flow Establishment (ZOFE) [e.g., *Albertson et al*., 1950; *Rajaratnam*, 1976]. Deeper within the pool, the jet decelerates in a zone referred to as the Zone of Established Flow (ZOEF) (Figure 2).

We calculate plunge-pool bed shear stress, τ_{pool}, where the waterfall jet impinges on the plunge-pool floor following the framework of *Stein et al*. [1993]. Within the jet-descending region, τ_{pool} is calculated as

$$\tau_{pool} = \rho C_{f\_pool} u_{impact}^2, \tag{1}$$

where C_{f_pool} is an empirical friction factor for the pool, ρ is fluid density, and u_{impact} is the waterfall jet velocity at impact with the plunge-pool floor. u_{impact} depends on whether the jet is within the ZOEF or ZOFE, such that calculating u_{impact} first requires an estimate of the length scale of the ZOFE, λ, which is commonly represented as [e.g., *Stein et al*., 1993]

$$\lambda = 2C_d^2 r_{jet} \sin\beta. \tag{2}$$

Here C_d is a diffusion constant empirically found to be ~2.6 for plunge pools [*Beltaos and Rajaratnam*, 1973; *Beltaos*, 1976], r_{jet} is the waterfall jet radius, and β is the jet impact angle with respect to the water surface (Figure 2). We calculate β from the water velocity at the waterfall brink, u_{brink}, and the waterfall drop height, H_{drop}; i.e.,

$$\beta = \tan^{-1}\left(\frac{\sqrt{2gH_{drop}}}{u_{brink}}\right), \tag{3}$$

where g is gravitational acceleration.

To calculate the jet radius, we assume a circular jet and apply conservation of mass for water flow (i.e., $Q_w = u_{jet}A_{jet}$, where Q_w is water discharge and u_{jet} and A_{jet} are the jet velocity and cross-sectional area at impact with the plunge-pool water surface, respectively) to solve for r_{jet} as

$$r_{jet} = \left(\frac{A_{jet}}{\pi}\right)^{1/2} = \left(\frac{Q_w}{\pi u_{jet}}\right)^{1/2}. \tag{4}$$

Using conservation of energy and neglecting jet breakup and energy losses due to air drag and wind, u_{jet} can be calculated as

$$u_{jet} = \sqrt{u_{brink}^2 + 2gH_{drop}}. \tag{5}$$

The jet centerline velocity within the plunge pool is constant in the ZOFE (i.e., for $z > z_\lambda$, where $z_\lambda = z_{water} - \lambda$ is the elevation at the boundary between the ZOFE and ZOEF and z_{water} is the elevation of the plunge-pool

water surface, Figure 2) and decreases with distance within the ZOEF (i.e., for $z < z_\lambda$). Jet impact velocity on the pool floor can be calculated following well-established theory as [e.g., *Albertson et al.*, 1950; *Stein et al.*, 1993]

$$u_{\text{impact}} = u_{\text{jet}} \quad \text{for} \quad z_{\text{sed}} > z_\lambda, \tag{6a}$$

$$u_{\text{impact}} = u_{\text{jet}} \sqrt{\frac{\lambda}{z_{\text{water}} - z_{\text{sed}}}} \quad \text{for} \quad z_{\text{sed}} < z_\lambda. \tag{6b}$$

Note that if no sediment is deposited on the pool floor, $z_{\text{sed}} = z_{\text{BR}}$, where z_{BR} is the elevation of the bedrock pool floor.

By combining equations (1) to (6a) and (6b), plunge-pool bed shear stress can be calculated from upstream flow conditions (u_{brink} and Q_w), waterfall plunge-pool geometry (z_{sed} and H_{drop}), tailwater elevation (z_{water}), and constants (C_{f_pool}, C_d, and g) as

$$\tau_{\text{pool}} = \rho C_{f\_\text{pool}} \left(u_{\text{brink}}^2 + 2gH_{\text{drop}}\right) \quad \text{for} \quad z_{\text{sed}} > z_\lambda, \tag{7a}$$

$$\tau_{\text{pool}} = \rho C_{f\_\text{pool}} \left(u_{\text{brink}}^2 + 2gH_{\text{drop}}\right) \left[2C_d^2 \frac{{Q_w}^{1/2}}{\left(\pi \sqrt{u_{\text{brink}}^2 + 2gH_{\text{drop}}}\right)^{1/2} (z_{\text{water}} - z_{\text{sed}})} \sin\left(\tan^{-1}\left[\sqrt{2gH_{\text{drop}}}/u_{\text{brink}}\right]\right) \right] \quad \text{for} \quad z_{\text{sed}} < z_\lambda. \tag{7b}$$

Calculating τ_{pool} requires an estimate of the flow velocity at the waterfall brink, which can be solved for straight 1-D escarpments following established theory [*Rouse*, 1936, 1937b; *Hager*, 1983] as

$$u_{\text{brink}} = u_n \left(\frac{0.4 + Fr_n^2}{Fr_n^2}\right) \quad \text{for} \quad Fr_n > 1, \tag{8a}$$

$$u_{\text{brink}} = u_n \left(\frac{1.4}{Fr_n^{2/3}}\right) \quad \text{for } Fr_n < 1. \tag{8b}$$

Fr_n and u_n in equation (8) are the Froude number and flow velocity, respectively, under the assumption of normal (steady and uniform) flow, which is assumed to occur upstream of the waterfall. Fr_n is the ratio of water velocity relative to the shallow-water wave speed and is defined as

$$Fr_n \equiv \frac{u_n}{\sqrt{gh_n}}, \tag{9}$$

where h_n is the normal flow depth upstream (Figure 2). Due to the normal flow assumption (i.e., $\tau_{\text{river}} = \rho g h_n S = \rho C_{f\_\text{river}} u_n^2$, where τ_{river} and C_{f_river} are the river bed shear stress and friction factor, respectively, and S is channel slope), Fr_n can also be represented by the ratio of S and C_{f_river} as

$$Fr_n = \sqrt{\frac{S}{C_{f\_\text{river}}}}. \tag{10}$$

For horseshoe-shaped waterfalls where flow converges laterally, equations (8a) and (8b) can be replaced with the theory of *Lapotre and Lamb* [2015].

Finally, to apply equation (7b), we need to constrain the elevation of the water surface in the pool, z_{water}, which we do using mass balance at the downstream plunge-pool lip. The depth of flow at the downsteam lip, $z_{\text{water}} - z_{\text{lip}}$, can be found by conserving mass for water overflow (i.e., $Q_w = u_{\text{lip}} W [z_{\text{water}} - z_{\text{lip}}]$, where W is reach-averaged channel width and u_{lip} is the water velocity at the downstream plunge-pool lip, Figure 2), and assuming a Froude number of unity at the downstream plunge-pool lip [*Chow*, 2009], such that

$$\left(z_{\text{water}} - z_{\text{lip}}\right) = \left(\frac{Q_w}{W\sqrt{g}}\right)^{2/3}, \tag{11}$$

equation (11) can be solved for z_{water} using a value for z_{lip} (which is assumed to be known).

By combining equations (7) through (11) and conserving mass ($Q_w = u_n W h_n$), τ_{pool} can be calculated from five field-measurable variables (h_{pool}, H_{drop}, Q_w, S, and W) and six constants (C_d, C_{f_pool}, C_{f_river}, g, ρ, and π), where pool depth is calculated by definition as $h_{pool} = z_{lip} - z_{sed}$.

All six of these constants above are known or have been specified above except for the friction factors within the pool and the river section. Many empirical relations exist to estimate C_{f_river} [e.g., *Garcia*, 2008], with relationships often based on ratios of channel roughness or grain size (D) to flow depth [e.g., *Parker*, 1991], e.g.,

$$C_{f\_river} = \left[8.1(h_n/D)^{(1/6)}\right]^{-2}. \tag{12}$$

Parker [2008] compiled data for sand and gravel-bedded streams showing C_{f_river} tends to be around ~10^{-2} to 10^{-3}. Less work has been done to estimate the plunge-pool friction factor. *Stein et al*. [1993] estimate C_{f_pool} to be a function of waterfall jet Reynolds number, but most natural waterfalls should be fully turbulent such that C_{f_pool} should be independent of the Reynolds number. Modifying equation (12) for plunge pools (i.e., $C_{f\_pool} = [8.1([z_{water} - z_{sed}]/D)^{(1/6)}]^{-2}$) yields C_{f_pool} estimates of order 10^{-3} using plunge-pool depth and grain size measurements we surveyed in the field (section 4 and Table S1 in the supporting information). For simplicity, we set $C_{f\_pool} = 10^{-3}$.

3.2. Jet Spreading and Return Flow

Diffusion of the waterfall jet into the surrounding water within the ZOEF results in a reduction in jet velocity and an increase in jet planform area [e.g., *Albertson et al*., 1950; *Rajaratnam*, 1976]. Experimental work has shown that within the ZOEF turbulent jets are characterized by self-similar velocity profiles [e.g., *Abramovich and Schindel*, 1963; *Giger et al*., 1991; *Rowland et al*., 2009]. Radial jet spreading with distance into the ZOEF is typically described by the length of its half-width, $b(z)$, which represents the radial distance at which the jet velocity has dropped to one half of the jet centerline velocity. Within the ZOEF ($z < z_\lambda$), we assume the half-width increases with increasing distance along the jet centerline following existing theoretical expectations and experimental observations [e.g., *Abramovich and Schindel*, 1963; *Giger et al*., 1991], such that

$$b(z) \approx 0.1(z_{water} - z - \gamma) \quad \text{for} \quad z < z_\lambda, \tag{13a}$$

where γ is a virtual origin which we assume is equal to zero. The half-width is less sensitive to distance within the ZOFE ($z > z_\lambda$) [e.g., *Albertson et al*., 1950], such that we assume a constant half-width within this zone based on the half-width at $z = \lambda$

$$b(z) \approx 0.1(z_{water} - z_\lambda - \gamma) \quad \text{for} \quad z > z_\lambda. \tag{13b}$$

For jets that impact the plunge-pool water surface at near vertical angles, equation (13b) reduces to $b(z > z_\lambda) \approx 1.4 r_{jet}$. At radial distances of $r > 2b(z)$ the jet velocity approaches that of the surrounding fluid, and we define the extent of the jet-descending region to be a vertically-oriented cylinder of radius $\delta = 2b(z = z_{sed})$ centered on the point of jet impingement on the plunge pool floor (Figure 2).

We define the jet return-flow region at radial distances $\delta < r < r_{pool}$, where r_{pool} is the plunge-pool radius. We assume water flows upwards in this region, providing a net upward directed current that aids transport of sediment out of the plunge pool (Figure 2). We estimate the upward velocity within the jet return-flow region, w_{up}, from conservation of mass as

$$w_{up} = \frac{Q_w}{(A_{pool} - A_{jet})}, \tag{14}$$

where $A_{pool} = \pi {r_{pool}}^2$ is the plunge-pool cross-sectional area. Equation (14) represents a plunge pool averaged estimation, assuming w_{up} is not a function of z and r. Note that equation (14) uses the jet radius at z_{water} rather than a radius based on the size of the jet within the pool to better characterize upward flow velocity near the top of the plunge pool, which will be shown to be important to determine sediment flux out of the pool.

3.3. Plunge-Pool Sediment Concentration

Conservation of suspended sediment at steady state can be written in terms of volumetric sediment concentration, c, within the jet return-flow region as

$$\frac{1}{r}\frac{\partial}{\partial r}(r u_r c) + \frac{1}{r}\frac{\partial}{\partial \theta}(u_\theta c) + \frac{\partial}{\partial z}\left(\left[w_{up} - w_s\right]c\right) = 0. \tag{15}$$

Here θ is an azimuthal coordinate, u_r and u_θ represent flow velocities in the radial and azimuthal directions, respectively, and w_s is particle terminal settling velocity (positive in the downward direction) calculated for dilute flow following *Ferguson and Church* [2004]

$$w_s = \frac{RgD^2}{a_1 v + \sqrt{0.75 a_2 RgD^3}}. \tag{16}$$

$R = (\rho_s - \rho)/\rho$ is the submerged specific sediment density, ρ_s is the sediment density, v is the kinematic fluid viscosity, and $a_1 = 20$ and $a_2 = 1.1$ are empirical constants. We define the net particle settling velocity as $w_{\text{net}} = w_s - w_{\text{up}}$ which represents the difference between the particle gravitational settling velocity and the upward return flow.

Decomposing velocities and sediment concentration into temporal averages (denoted by overbars) and fluctuating components (denoted by prime marks), (i.e., $u_r(r,t) = \overline{u_r(r)} + u_r(r,t)'$, $w_{up}(t) = \overline{w_{up}} + w_{up}(t)'$, and $c(r,z,t) = \overline{c(r,z)} + c(r,z,t)'$, where t is time (i.e., Reynolds decomposition)), neglecting the mean radial velocity based on our assumption of purely vertical flow (i.e., $\overline{u_r(r)} = 0$), and assuming axisymmetric flow (i.e., $\partial/\partial\theta = 0$) reduce equation (15) to

$$\frac{1}{r}\frac{\partial}{\partial r}\left(r\overline{u_r' c'}\right) + \frac{\partial}{\partial z}\left(\overline{w_{\text{up}}' c'}\right) - w_{\text{net}}\frac{\partial \overline{c}}{\partial z} = 0. \tag{17}$$

Equation (17) states that variation in sediment concentration throughout the plunge pool is set by a balance between turbulent diffusion and particle settling. Neglecting radial advection in equation (17) is partially supported by a recent study showing turbulent kinetic energy better predicts sediment scour from plunge pools compared to bed shear stress from radial jets along the pool floor [*Ghaneeizad et al.*, 2015]. Solving equation (17) throughout the plunge pool requires applying boundary conditions that are difficult to determine. As plunge-pool sediment-transport capacity is sensitive to sediment concentration at the downstream plunge-pool lip, we solve for sediment concentration only along boundaries at the pool floor and along the walls. Similar in concept to a bed load layer [e.g., *McLean*, 1992], we assume there exists a thin layer of well-mixed sediment along the plunge-pool floor and define z_{mixed} as the elevation of the top of this layer (Figure 2). We define sediment concentration along boundaries at the pool wall ($r = r_{\text{pool}}$, $z_{\text{mixed}} < z < z_{\text{water}}$) and at the top of the mixed layer near the pool floor within the jet return-flow region ($\delta < r < r_{\text{pool}}$, $z = z_{\text{mixed}}$).

There is no radial flux of sediment through the plunge-pool walls, such that at the boundary $r = r_{\text{pool}}$ equation (17) reduces to

$$\frac{\mathrm{d}}{\mathrm{d}z}\left(\overline{w_{\text{up}}' c'\left(r_{\text{pool}}, z\right)}\right) - w_{\text{net}}\frac{\mathrm{d}\overline{c\left(r_{\text{pool}}, z\right)}}{\mathrm{d}z} = 0. \tag{18}$$

Equation (18) is technically only valid at $z < z_{\text{lip}}$ because radial fluxes at $z_{\text{lip}} < z < z_{\text{water}}$ are responsible for transporting sediment out of the pool; however, for pools that are deep relative to the tailwater depth ($[z_{\text{lip}} - z_{\text{sed}}] >> [z_{\text{water}} - z_{\text{lip}}]$), equation (18) should be a reasonable approximation. Equation (18) represents a balance between net particle settling and turbulent diffusion similar to classic descriptions of sediment suspension for shear flows [e.g., *Rouse*, 1937a]. We represent the turbulent flux of sediment using an eddy viscosity, v_e, assumed to be constant within the plunge pool

$$\overline{w_{\text{up}}' c'\left(r_{\text{pool}}, z\right)} = -v_e\frac{\mathrm{d}\overline{c\left(r_{\text{pool}}, z\right)}}{\mathrm{d}z}. \tag{19}$$

Substituting equation (19) into (18) and integrating under the condition of zero net vertical sediment flux at the water surface yields

$$\frac{\mathrm{d}\overline{c\left(r_{\text{pool}}, z\right)}}{\mathrm{d}z} = -\frac{w_{\text{net}}}{v_e}\overline{c\left(r_{\text{pool}}, z\right)} = -\frac{\overline{c\left(r_{\text{pool}}, z\right)}}{L_d}. \tag{20}$$

The quantity $v_e/w_{\text{net}} \equiv L_d$ represents a length scale over which turbulence mixes sediment, similar in concept to a diffusion length scale. We solve for $\overline{c\left(r_{\text{pool}}, z\right)}$ by integrating equation (20) and applying the boundary

condition of a known reference sediment concentration at the top of the well-mixed layer, $\overline{c(r_{\text{pool}}, z_{\text{mixed}})} = c_0$. Assuming L_d is not a function of z, this integration yields

$$\overline{c(r_{\text{pool}}, z)} = c_0 \exp\left(-\frac{(z - z_{\text{mixed}})}{L_d}\right). \tag{21}$$

To find c_0 in equation (21), we solve for sediment concentration at the top of the well-mixed layer within the jet return-flow region (i.e., $\delta < r < r_{\text{pool}}$ and $z = z_{\text{mixed}}$). Following our conceptualization in Figure 2, there is no entrainment of sediment from the bed within the jet return-flow region, and we neglect all vertical fluxes except for settling, such that equation (17) reduces to

$$\frac{1}{r}\frac{\mathrm{d}}{\mathrm{d}r}\left(r\overline{u_r' c'(r, z_{\text{mixed}})}\right) - w_{\text{net}}\frac{\mathrm{d}\overline{c(r, z_{\text{mixed}})}}{\mathrm{d}z} = 0. \tag{22}$$

We represent turbulent mixing of sediment with an eddy viscosity as in equation (19); i.e.,

$$\overline{u_r' c'(r, z_{\text{mixed}})} = -v_e \frac{\mathrm{d}\overline{c(r, z_{\text{mixed}})}}{\mathrm{d}r}. \tag{23}$$

Substituting equation (23) into (22), and, for simplicity, assuming that v_e is not a function of r, yields

$$\frac{\mathrm{d}^2\overline{c(r, z_{\text{mixed}})}}{\mathrm{d}r^2} + \frac{1}{r}\frac{\mathrm{d}\overline{c(r, z_{\text{mixed}})}}{\mathrm{d}r} + \frac{w_{\text{net}}}{v_e}\frac{\mathrm{d}\overline{c(r, z_{\text{mixed}})}}{\mathrm{d}z} = 0. \tag{24}$$

Equation (24) is a second-order linear partial differential equation which we solve using separation of variables and by applying boundary conditions of no sediment flux at the plunge-pool walls, known sediment concentration, c_b, at the boundary between the jet-descending and return-flow regions, and that sediment concentration must match where the top of the mixed layer meets the pool wall at (r_{pool}, z_{mixed})

$$\frac{\mathrm{d}\overline{c(r_{\text{pool}}, z_{\text{mixed}})}}{\mathrm{d}r} = 0, \tag{25a}$$

$$\overline{c(\delta, z_{\text{mixed}})} = c_b, \tag{25b}$$

$$\overline{c(r_{\text{pool}}, z_{\text{mixed}})} = c_0. \tag{25c}$$

Solving equation (24) with the boundary conditions specified in equations (25a), (25b), (25c) yields

$$\overline{c(r, z_{\text{mixed}})} = c_b\left(\frac{I_0(r/L_d) + \frac{I_1(r_{\text{pool}}/L_d)}{K_1(r_{\text{pool}}/L_d)}K_o(r/L_d)}{I_0(\delta/L_d) + \frac{I_1(r_{\text{pool}}/L_d)}{K_1(r_{\text{pool}}/L_d)}K_0(\delta/L_d)}\right). \tag{26}$$

I_0, K_0, I_1, and K_1 in equation (26) are the modified Bessel functions of the first and second kind of order 0 and 1, respectively, and appear in equation (26) due to the cylindrical geometry imposed. Formulating the same problem in a rectangular geometry would yield a solution with cross-stream exponential decay of sediment concentration, analogous to that used by *Pizzuto* [1987], and may be more appropriate for waterfalls with wide, curtain-like jets. Note that equation (26) is derived specifically for the bottom boundary of the jet return-flow region and should hold for $r > \delta$. For $r < \delta$ we set $\overline{c(r, z_{\text{mixed}})} = c_b$ under the assumption that sediment concentration is well mixed with respect to r within the jet-descending region.

Finally, combining equations (21), (25c), and (26) yields our final equation to predicted sediment concentration along the plunge-pool wall

$$\overline{c(r_{\text{pool}}, z)} = c_b \exp\left(-\frac{(z - z_{\text{mixed}})}{L_d}\right)\left(\frac{I_0(r_{\text{pool}}/L_d) + \frac{I_1(r_{\text{pool}}/L_d)}{K_1(r_{\text{pool}}/L_d)}K_o(r_{\text{pool}}/L_d)}{I_0(\delta/L_d) + \frac{I_1(r_{\text{pool}}/L_d)}{K_1(r_{\text{pool}}/L_d)}K_0(\delta/L_d)}\right). \tag{27}$$

Note that when $L_d < 0$ (which can occur if $w_{\text{net}} < 0$; i.e., upward advective velocity is greater than particle gravitational settling), we set $\overline{c(r_{\text{pool}}, z)} = c_b$; i.e., sediment is well-mixed throughout the pool. Additionally, when $z < z_{\text{mixed}}$ (i.e., for pool depths shallower than the mixed layer thickness), we set the exponential term in equation (27) to unity.

To apply equation (27), we must specify v_e, z_{mixed}, and c_b. Following the approach of *Prandtl* [1925], we assume v_e scales with turbulent fluctuations on the plunge-pool floor, which we represent with the plunge-pool shear velocity at the bed, u_{*pool}, as is commonly observed in open-channel flows [e.g., *Nezu and Nakagawa*, 1993], and a mixing length scale over which the impinging jet diffuses into the pool, for which we use λ, resulting in

$$v_e = k_1\left(\tau_{pool}/\rho\right)^{1/2}\lambda = k_1 u_{*pool}\lambda. \tag{28}$$

Here k_1 is a coefficient which we set equal to unity. Similar Prandtl-type approaches have been applied to turbulent jets [e.g., *Albertson et al.*, 1950; *Abramovich and Schindel*, 1963; *Bradbury*, 1965]. These studies typically use a turbulent mixing length related to the jet half-width as they are primarily interested in describing the lateral spread of the jet within the ZOEF, whereas we wish to characterize both the radial and vertical turbulence throughout the plunge pool. Using a mixing length related to jet half-width instead of λ affects the absolute magnitude, but not the trends, of plunge-pool sediment-transport capacity predictions presented below.

We assume the height of the well-mixed zone of sediment near the pool floor extends to the peak saltation height of bed load particles and estimate z_{mixed} with the empirical formula from *Sklar and Dietrich* [2004] for noncohesive particles with large particle Reynolds numbers, i.e., $z_{mixed} = 1.44D(\tau_{*pool}/\tau_{*c} - 1)^{0.5} + z_{sed}$. τ_{*c} is the nondimensional critical Shields stress for incipient grain motion which is observed to be approximately constant (i.e., $\tau_{*c} = 0.045$) for gravel-sized particles and larger [*Buffington and Montgomery*, 1997]. The critical Shields stress for finer sediment can be found from *Brownlie* [1981]. τ_{*pool} is the nondimensional Shields stress at the base of the plunge pool and is defined as

$$\tau_{*pool} = \frac{\tau_{pool}}{(\rho_s - \rho)gD}. \tag{29}$$

Following standard sediment entrainment theory [e.g., *van Rijn*, 1984], we assume that for plunge pools at steady-state depths the near-bed sediment concentration equals the dimensionless sediment entrainment rate, which scales with plunge-pool transport stage (τ_{*pool}/τ_{*c}) as

$$c_b = k_2\left(\frac{\tau_{*pool}}{\tau_{*c}} - 1\right)^{1.5}. \tag{30}$$

For cases where $\tau_{*pool} < \tau_{*c}$, there is no sediment entrainment and $c_b = 0$. For very high transport stages c_b can grow to unreasonable values and it is appropriate to apply a limit [e.g., *Garcia and Parker*, 1991]; here we set a maximum value of $c_b = 0.2$. k_2 in equation (30) is an empirical parameter which varies in existing literature. *Van Rijn* [1984] suggests that k_2 is a function of grain size and ranges from $\sim 10^{-4} < k_2 < \sim 10^{-2}$. Rearranging standard bed load transport models [e.g., *Fernandez Luque and van Beek*, 1976] to yield estimates of near-bed sediment concentration gives $\sim 10^{-3} < k_2 < \sim 10^{-1}$ depending on flow conditions. We set $k_2 = 0.02$, which is within these previous estimates and provides a good match to our experimental data (section 6).

Figure 3 shows profiles of sediment concentration along the pool floor and walls normalized by near-bed concentration for an example waterfall plunge pool. Note that $\overline{c(r, z_{mixed})}/c_b$ is set to be unity for $r < \delta$; this area represents well-mixed sediment within the jet-descending region. $\overline{c(r_{pool}, z)}/c_b$ is also constant for $z < z_{mixed}$ due to our assumption of well-mixed sediment near the plunge-pool floor. The combination of decay of sediment concentration with increasing radial and vertical distance from the point of jet impingement results in the plunge-pool lip having the lowest sediment concentration.

3.4. Plunge-Pool Sediment-Transport Capacity

For alluvial-floored pools, we define plunge-pool sediment-transport capacity (Q_{sc_pool}) as the flux of sediment transported out of the plunge pool to the river reach immediately downstream and calculate Q_{sc_pool} as the product of water discharge (Q_w) and the average sediment concentration at the downstream plunge-pool lip, i.e.,

$$Q_{sc\_pool} = \frac{Q_w}{\left(z_{water} - z_{lip}\right)}\int_{z=z_{lip}}^{z=z_{water}} \overline{c\left(r_{pool}, z\right)}\,dz. \tag{31}$$

For plunge pools that have large depths relative to the tailwater depth, equation (31) can be approximated by

$$Q_{sc\_pool} = Q_w\overline{c\left(r_{pool}, z_{lip}\right)}. \tag{32}$$

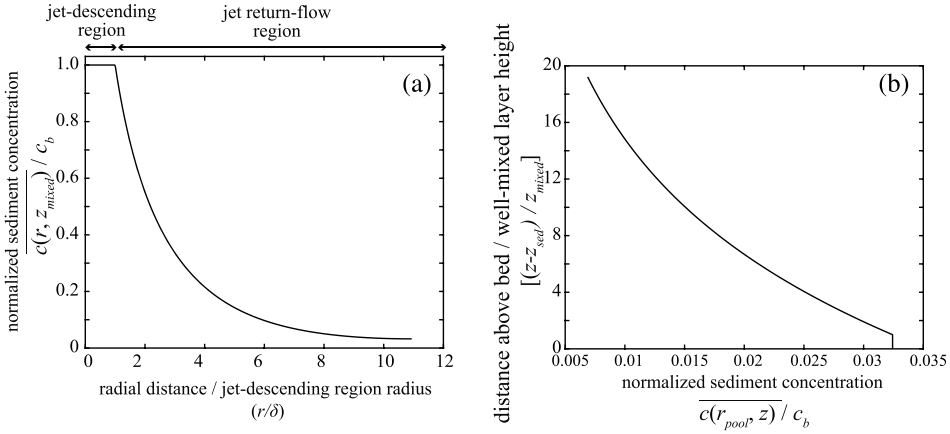

Figure 3. Profiles of (a) radial and (b) vertical sediment concentration normalized by near-bed concentration in the jet-descending region (c_b). Figure 3a depicts normalized sediment concentration near the plunge-pool floor at $z = z_{mixed}$, and Figure 3b shows normalized sediment concentration along the plunge-pool wall at $r = r_{pool}$. Parameters for this calculation based on Lower Switzer Falls, Arroyo Seco, California (LSF, Table S1); water discharge of 4.8 m^3/s, waterfall drop height of 5 m, grain size of 0.1 m, plunge-pool radius (r_{pool}) of 4.4 m, and upstream normal Froude of 1.9. δ = radius of jet-descending region; z_{mixed} = elevation of the top of the well-mixed layer near the pool floor.

Our model indicates that the plunge-pool sediment-transport capacity, Q_{sc_pool}, can be calculated from seven field-measurable variables (Q_w, r_{pool}, h_{pool}, D, H_{drop}, S, and W) and 13 constants (C_{f_river}, C_{f_pool}, C_d, a_1, a_2, g, k_1, k_2, γ, ν, π, ρ, and ρ_s) from equations (7) through (11), (13), (14), (16), and (27) through (31). Due to the exponential and modified Bessel function terms in equation (27), Q_{sc_pool} only goes to zero in the limit when z or r go to infinity, or when $c_b = 0$. Following standard practice for bed load transport threshold of motion, we set $Q_{sc\_pool} = 0$ when sediment flux falls below a dimensionless reference level ($Q_{sc\_pool} = 0$ for $Q_{*s\_pool} < 2 \times 10^{-5}$, where $Q_{*s\_pool} = Q_{sc\_pool}/(2r_{pool}RgD^3)^{1/2}$ is the dimensionless sediment flux) [e.g., *Parker et al.*, 1982].

3.5. Nondimensionalization

Inspection of equations (27), (30), and (32) shows that dimensionless plunge-pool sediment-transport capacity, Q_{sc_pool}/Q_w, can be predicted from four nondimensional variables

$$\frac{Q_{sc\_pool}}{Q_w} = \overline{c(r_{pool}, z_{lip})} = f\left(\frac{\tau*_{pool}}{\tau*_c}, \frac{(z_{lip} - z_{mixed})}{L_d}, \frac{r_{pool}}{L_d}, \frac{\delta}{L_d}\right). \quad (33)$$

$\tau*_{pool}/\tau*_c$ is the plunge-pool transport stage. Entrainment of sediment from the plunge-pool floor only occurs when $\tau*_{pool}/\tau*_c > 1$; however, unlike standard low-gradient river bed load transport models [e.g., *Meyer-Peter and Mueller*, 1948], $\tau*_{pool}/\tau*_c > 1$ is a necessary but insufficient condition for $Q_{sc\_pool} > 0$. This is because sediment transport out of the waterfall plunge pool requires both entrainment of particles from the plunge-pool floor and suspension of particles over the plunge-pool lip.

Suspension of sediment out of the plunge pool is governed by the remaining three nondimensional terms in equation (33). The term $(z_{lip} - z_{mixed})/L_d$, which is approximately equal to h_{pool}/L_d for deep pools, governs the vertical distribution of sediment concentration, such that when L_d is large relative to $(z_{lip} - z_{mixed})$ sediment is efficiently mixed in the vertical direction, resulting in higher sediment concentrations at the top of the plunge pool, and larger sediment transport capacities. Both r_{pool}/L_d and δ/L_d characterize the radial distribution of sediment concentration but work in opposite ways. Large values of r_{pool} relative to L_d indicate that the plunge pool is wide compared to the turbulent mixing length scale, resulting in lower sediment concentrations at the pool walls and smaller Q_{sc_pool}. In contrast, large values of δ relative to L_d indicate that the size of the jet-descending region, from which the jet entrains sediment, is the dominant scale influencing lateral sediment concentration, resulting in increased sediment concentration and transport capacity. $(z_{lip} - z_{mixed})/L_d$, r_{pool}/L_d, and δ/L_d are all functions of the same 7 independent variables and 13 constants specified in section 3.4.

3.6. Equilibrium Pool Depth

Finally, while equations (31) and (32) allow us to predict the sediment-transport capacity for a given pool depth (without any assumption of steady state), it can also be used to predict the steady-state pool depth for a given

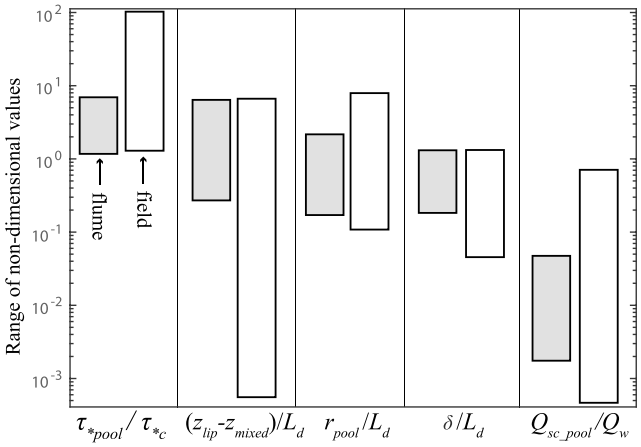

Figure 4. Comparison of range of nondimensional variables influencing plunge-pool sediment-transport capacity from flume measurements (gray boxes, Table S2) versus field measurements (white boxes, Table S1). Note that field values of nondimensional variables were calculated using the median grain diameter deposited within the plunge pool and we set $C_{f\_river} = 0.01$ [*Parker*, 2008]. Nondimensional variables: τ_{*pool}/τ_{*c} = plunge-pool transport stage, $(z_{lip} - z_{mixed})/L_d$ = approximate plunge-pool depth (for deep pools) normalized by turbulent mixing length scale, r_{pool}/L_d = plunge-pool radius normalized by turbulent mixing length scale, δ/L_d = jet-descending region radius normalized by turbulent mixing length scale, and Q_{sc_pool}/Q_w = plunge-pool sediment-transport capacity normalized by water discharge.

sediment supply. To make this later prediction, we use sediment mass balance and assume a steady-state pool depth by setting Q_{sc_pool} equal to the upstream sediment supply and iteratively solve the model to find the equilibrium pool depth. If the predicted equilibrium pool depth is deeper than the bedrock pool floor, the pool should be free of sediment cover with the bedrock floor exposed.

4. Surveys of Natural Waterfalls

To help design the parameter space that will be explored experimentally, we compiled data from a number of waterfalls and estimated the ranges for the dimensionless variables in equation (33). Our field survey focused on waterfalls within the San Gabriel Mountains, California, and also included waterfalls in the Sierra Nevada, California, and on the island of Kauai, Hawaii. These three field localities cover a range of sediment supply regimes, where sediment supply is high in the San Gabriel Mountains due to high erosion rates (~0.1–1 mm/yr [*DiBiase et al.*, 2010]) and frequent wildfires [e.g., *Lamb et al.*, 2011]. In contrast, a strong rainfall gradient creates variable sediment supply across the waterfalls we surveyed in Kauai [*Ferrier et al.*, 2013], and sediment supply is likely low in the Sierra Nevada due to erosion rates which are approximately 1–2 orders of magnitude lower (~0.02 mm/yr) than that observed in the San Gabriel Mountains [e.g., *Stock et al.*, 2005]. All surveyed waterfalls had clearly defined bedrock steps and ranged in drop height from 1 to 120 m, in plunge-pool bedrock radius from 0.5 to 40 m, and had upstream drainage areas ranging from < 1 to 94 km^2 (Table S1).

We surveyed pools during periods of low flow as waterfalls are often inaccessible and hazardous to survey during large flood events. The vast majority of surveyed pools were filled or partially filled with sediment during our field campaign, with pool depths ranging from 0 m (i.e., completely filled with sediment) to 5 m. For consistency with our theory developed above and our experimental measurements below, field pool depth was defined as the vertical distance between the downstream plunge-pool lip and the pool floor (i.e., $h_{pool} = z_{lip} - z_{sed}$). We estimated plunge-pool depth using a variety of methods (see supporting information S1 and Table S1). Grain size was estimated visually in the field or via a random-walk Wolman pebble count (comprising 50 to 100 grains and ignoring grains with $D < 2$ mm). Channel slope upstream of the waterfall was taken from digital elevation models ranging in resolution from 1 m lidar (most of the San Gabriel Mountain locations) to 10 m National Elevation Dataset data. We estimated water discharge using 2 year recurrence interval discharge values taken from U.S. Geological Survey stream gages located either within the same catchment as our field surveyed waterfall or within an adjacent catchment. We assumed a linear scaling between discharge and drainage area to convert discharge values taken at stream gage locations to waterfall locations. The range in dimensionless variables that emerge from our theory is given in Figure 4.

5. Experimental Methods

5.1. Experiment Design and Scaling

We designed laboratory flume experiments in order to test the quantitative predictions of our plunge-pool sediment-transport capacity model. We systematically and independently varied waterfall drop height, water discharge, grain size, and plunge-pool radius in order to observe their effects on plunge-pool sediment

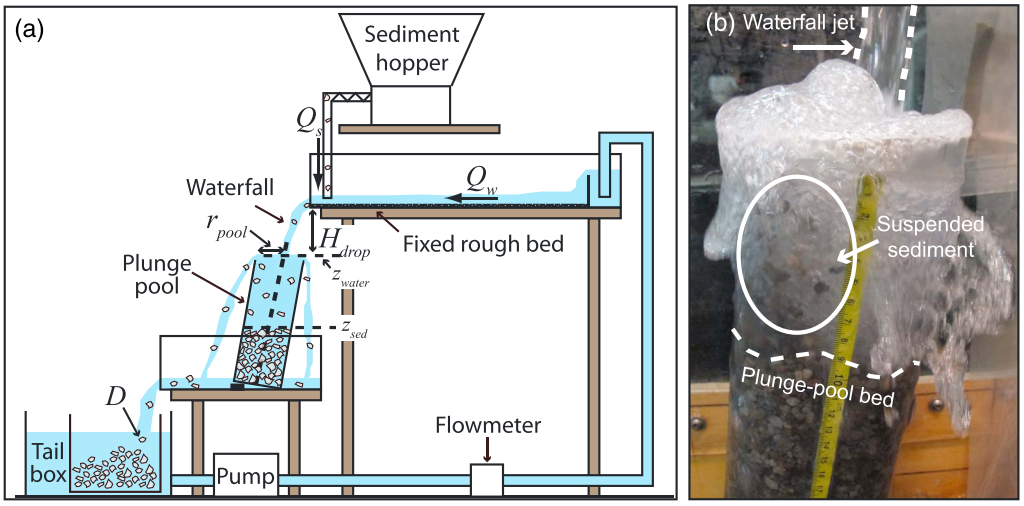

Figure 5. (a) Flume schematic with key variables labeled (D = grain size, H_{drop} = waterfall drop height, r_{pool} = plunge-pool radius, Q_s = sediment supply, Q_w = water discharge, z_{sed} = elevation of plunge-pool alluvial floor, and z_{water} = elevation of plunge-pool water surface). (b) Example photo of sediment transport through a waterfall plunge pool during experiment 12 (Table S2). Plunge pool is 10.2 cm in diameter, and yellow tape is marked in centimeter increments for scale.

transport capacity and pool depth. We attempted to achieve dynamic similarity with natural waterfalls by keeping flow Froude supercritical and in the fully turbulent regime [*Lamb et al.*, 2015]. Flow Reynolds numbers for our experiments varied between ~4000 and 5000 at the upstream waterfall brink, and particle Reynolds numbers ranged from ~1000 to 4000 depending on flow discharge and grain size. Froude numbers at the waterfall brink ranged from ~1.5 to 2, similar to what is expected for mountain rivers during floods [e.g., *Tinker and Wohl*, 1998; *Valle and Pasternack*, 2006].

Over 10 experimental sets, we produced 50 different pools with different steady-state pool depths, each with a unique combination of dimensional variables (Table S2). Ideally, we would design experiments to vary a single parameter in nondimensional space; however, the transient self-adjustment of plunge-pool depth to reach a new equilibrium in response to changing sediment supply made this logistically challenging as all our nondimensional parameters (i.e., equation (33)) are functions of pool depth. Instead, we designed experiments so that the range of dimensionless variables explored overlapped in nondimensional space with our measurements from natural waterfalls (Figure 4 and Table S1). Although our experimental waterfalls are smaller than natural waterfalls, the overlap in nondimensional space should allow the dynamics in the experiments to be comparable to those in natural waterfalls [e.g., *Lamb et al.*, 2015].

5.2. Experiment Setup and Methods

Our experimental setup (Figure 5) consisted of a 9.6 cm wide and 2.06 m long upstream flume with a fixed rough bed of 2.4 mm subrounded quartz grains. The upstream flume was raised and cantilevered over a downstream flume (24 cm wide by 80 cm long) forming a waterfall where a fully ventilated jet cascaded off the upstream flume and into a plunge pool positioned within the downstream flume. Water and sediment spilled out from the plunge pool and eventually into a tailbox from which a pump drew water to supply upstream. We designed our experiments to explore plunge-pool dynamics without complications from the downstream river sediment-transport capacity (e.g., the formation of bars or ridges at the downstream plunge-pool lip [e.g., *Pagliara et al.*, 2008b]); thus, sediment transported out of the plunge pool was immediately evacuated from the system. A pipe flow meter (with accuracy ± 1.5%) measured water discharge, and we confirmed measurements by weighing the mass of water discharge collected in a bucket over 10 to 30 s increments. A rotating auger fed sediment from a hopper into the system immediately upstream of the waterfall brink, allowing sediment supply to be controlled independent of the upstream hydrodynamics (Figure 5). We calibrated the auger feed rate by placing a mesh-bottomed bucket in the waterfall jet and weighing the mass of drained sediment collected over 60 s increments.

Unlike previous experiments which developed scour holes into loose sediment beds [*Stein and Julien*, 1993; *Lenzi and Comiti*, 2003; *Pagliara et al.*, 2006], we used clear, cylindrical PVC tubes ranging from ~10 to 20 cm

diameter as artificial plunge pools (Figure 5b). These rigid pipes simulated vertical bedrock-walled plunge pools, allowed for fluctuating levels of pool depths (e.g., Figures 1 and 2), and were sufficiently deep so that the alluvial floor was free to self-adjust without hitting the pipe bottom. We placed these smooth-walled tubes within the downstream flume and aligned the pipes so that the waterfall jet impacted the center of the tube. The angle of jet impact on the plunge-pool surface was dictated by the water discharge and waterfall drop height and was typically at angles of ~80° relative to horizontal; we back-tilted the PVC tubes by ~10° to force impingement perpendicular to the plunge-pool walls. We also affixed 10° wedges to the top of the tubes larger than 15 cm in diameter so that, despite back tilting, plunge-pool tops remained approximately horizontal.

We inferred plunge-pool sediment-transport capacity by feeding sediment at a known rate from upstream and allowing the pool to transiently adjust its depth until reaching a steady state where sediment supply into the pool equaled sediment flux out. Therefore, by mass balance, the imposed upstream sediment supply was equal to the plunge-pool sediment-transport capacity for the given experimental conditions. Each experimental set began with a plunge pool filled with well sorted sediment and water. Imposing clear-water discharge caused the pool to transiently scour until reaching a steady-state depth where sediment no longer left the pool. After recording this depth, a small stepwise increase in sediment flux from upstream was imposed, which forced transient aggradation of the pool to a new steady-state depth. Steady-state pool depths following changes in imposed sediment flux were typically reached in < 1 min, and we waited until pool depths were constant over a period of ~5–10 min (~10–15 min total wait time) before changing the imposed sediment flux. We repeated this process with subsequent increases in sediment flux until the pool either filled to its lip with sediment or the feeder's maximum sediment flux was reached. For each steady-state pool depth, we measured the maximum, minimum, and average depth to the sediment bed by eye using a ruler; we use the difference between the maximum and minimum depths as a representation of uncertainty and measured pool depth as $h_{pool} = z_{lip} - z_{sed}$ for consistency with our theory and field measurements. We made pool depth measurements while the experiment was running (i.e., the dynamic depth (in the sense of *Pagliara et al*. [2006])) to prevent sediment suspended in the water column from settling onto the bed which would result in artificially shallow pool depths. At the end of the experimental set, we returned to clear-water discharge to confirm that the pool depth returned to the original equilibrium clear-water depth observed at the start.

6. Experimental and Theoretical Results

6.1. Sediment Transport Observations

For a typical experimental set, plunge pools that were initially filled with sediment rapidly scoured to deeper depths after turning on clear-water discharge. The rate of plunge-pool scour decreased as pools deepened and approached a steady-state depth. At steady state with clear-water discharge, sediment was mobilized from the bed but not suspended high enough to be transported over the plunge-pool walls.

Plunge-pool sediment transport occurred primarily via suspension of grains whereby the impinging jet created a small scour hole in the sediment bed from which grains were initially entrained. Scour holes were characterized by steep walls which acted as ramps, and mobilized grains would roll or saltate a short distance up this ramp before becoming suspended in the return flow of the jet (Figure 5b and Movie S1). Suspended grains were typically concentrated on the downstream side of the waterfall jet but were observed throughout the plunge pool. Grains were suspended in a mixture of water and air (with air entrained by the impinging jet) and were brought to the top of the water column and transported out of the pool as water spilled over the pool walls. Both the rate of sediment entrainment and the vigor with which the water, air, and sediment mixture boiled over the plunge-pool walls appeared to fluctuate over timescales of seconds, reflecting macroturbulence within the pool.

As increases in sediment supply forced plunge pools to aggrade to increasingly shallow equilibrium depths, the concentration of sediment in the water column and vigor with which grains were suspended visually increased and an active layer of sediment transport developed near the plunge-pool floor. This active layer visually was approximately five grain diameters thick and was defined by a zone of highly concentrated mobile grains below a more dilute layer. When pools aggraded within ~5 cm of the plunge-pool lip, the sediment bed appeared fluidized.

6.2. Influence of Sediment Supply and Pool Depth

In all our experiments, we observed plunge pools to transiently aggrade in response to stepwise increases in imposed sediment supply, with all other parameters held constant, until a new equilibrium pool depth was reached (Figure 6 and Table S2). The magnitude of pool aggradation between equilibrium depths was typically greatest when switching from clear-water discharge to a small sediment supply, with subsequent sediment supply increases resulting in moderate aggradation to reach a new equilibrium depth. An exception to this was for very shallow pools which had rapid, transient aggradation when depths were less than ~ 5 cm (e.g., Exp 9, Figure 6c). For all experiments, plunge-pool equilibrium depth under clear-water flow was the same at the start and end of the experiment set within measurement error. These results are consistent with our conceptual model in that, when all else is held constant, the pool depth adjusts to bring the sediment-transport capacity into equilibrium with the imposed sediment load, after which no aggradation occurs. Thus, these results implicitly show that, all else held constant, shallower pools at steady state have a higher sediment-transport capacity than deeper pools.

Our plunge-pool sediment-transport capacity model shows variability in its goodness of fit to the experimental data when setting the constant $k_2 = 0.02$ (solid lines in Figure 6). In all cases, the model predicts that sediment-transport capacity increases with decreasing equilibrium plunge-pool depth when all else is held constant, in agreement with our experiments. The relationship between equilibrium pool depth and sediment-transport capacity in the model is controlled by two main factors. First, sediment transport out of deeper pools requires grains to be suspended higher in the water column, resulting in reduced sediment concentration at the plunge-pool lip and, in turn, reduced values of Q_{sc_pool}. Second, within the ZOEF, τ_{pool} decreases with increasing pool depth, which in turn reduces both the entrainment of sediment from the pool floor (lower c_b) and the efficiency of turbulent mixing (smaller L_d). This second influence does not exist when $z_{sed} > z_\lambda$ because τ_{pool} is independent of pool depth in this regime (equation (7)), resulting in increased sensitivity between sediment supply and equilibrium pool depth (this transition, $z_{sed} = z_\lambda$, is marked by red stars in Figure 6).

6.3. Influence of Water Discharge, Waterfall Drop Height, and Grain Size

We explored the influence of changing waterfall drop height, water discharge, and grain size on pool depth by varying one of these parameters while holding all other variables constant. For the same imposed sediment load, plunge pools with greater water discharges in our experiments always had deeper equilibrium depths than those with smaller discharges (Figure 6a). Similarly, greater waterfall drop heights (Figure 6b) and finer grain sizes (Figure 6c) always led to deeper pool depths at equilibrium, all else held constant. Because these measurements were made for equilibrium pool depths, where sediment supply was equal to sediment-transport capacity, comparing experiments that produced the same equilibrium pool depths but under different sediment supply rates allows one to infer the controls on sediment-transport capacity. In this way, Figure 6 shows that for a given equilibrium pool depth, and all else held constant (except sediment supply), plunge-pool sediment-transport capacity increases with increasing waterfall drop height, increasing water discharge and decreasing grain size. While the theoretical predictions show variable success in matching sediment-transport capacity observations (17 of 40 theoretical predictions agree with experimental observations within measurement error in Figures 6a–6c), the theory does capture the experimental data trends.

Increases in water discharge and waterfall drop height both increase the total energy that is delivered to the plunge pool; however, changes in water discharge and drop height have distinct effects within our theoretical framework. All else being equal, increases in water discharge lead to nonlinear increases in Q_{sc_pool} in our model for three reasons. First, because Q_{sc_pool} is calculated as the product of sediment concentration at the plunge-pool lip and water discharge (equation (31)), increasing Q_w results in a direct increase in Q_{sc_pool} even for cases of constant sediment concentration. Second, w_{up} increases with water discharge due to both increased water flux and larger waterfall jet radii (which force the return flow through a smaller annulus) (equation (14)), resulting in reduced net particle settling velocities and higher sediment concentrations at the plunge-pool lip. Third, τ_{pool} increases with water discharge, which acts to increase both sediment entrainment (c_b) and turbulent mixing (L_d).

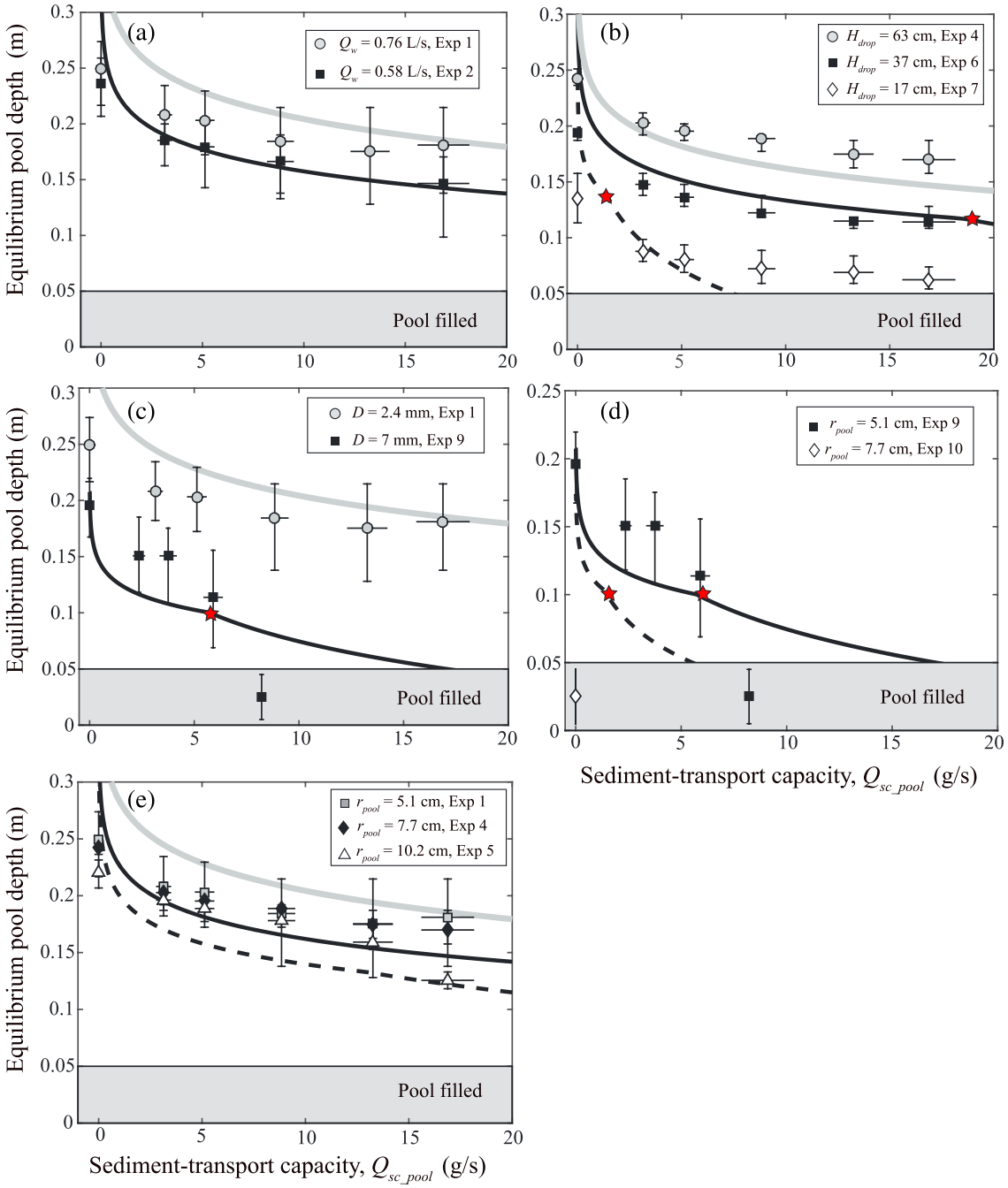

Figure 6. Experimental results (symbols) and model predictions (lines) for plunge-pool depth, h_{pool}, measured during equilibrium transport (where, due to steady-state pool depth conditions, the plunge-pool sediment-transport capacity, Q_{sc_pool}, is necessarily equal to the sediment supply by mass balance) for experiments varying (a) water discharge (Q_w), (b) waterfall drop height (H_{drop}), (c) grain size (D), (d) plunge-pool radius (r_{pool}) with 7 mm diameter sediment, and (e) plunge-pool radius with 2.4 mm diameter sediment, with all other dimensional variables held constant. Gray lines are predictions that correspond to the data represented by gray-filled markers; black lines correspond to black-filled markers, and dashed lines correspond to white-filled markers. See Table S2 for all experimental parameter values and results. Vertical error bars reflect topographic variability across the plunge-pool floor, and horizontal error bars show standard deviation of sediment supply measurements. Red stars indicate transition from ZOEF (above red star) to ZOFE (below red star). We classified the plunge pools with depths of ~ 0–5 cm as filled (gray box); we make no model predictions at these depths where we observed a change in process from grain suspension to fluidization of the bed (see section 6.1 for details).

Unlike increasing water discharge, which causes wider waterfall jets and larger w_{up} values, increasing H_{drop} causes waterfall jets to narrow and w_{up} to decrease (equations (4), (5), and (14)). Despite this effect, plunge-pool sediment-transport capacity still increases with waterfall drop height in our model framework due to the increase in waterfall jet velocity with H_{drop} (equation (5)). Higher jet velocity increases τ_{pool}, leading to enhanced sediment entrainment and increased turbulent mixing.

Increases in grain size decrease plunge-pool sediment-transport capacity in our model when all else is held constant due to the decrease in transport stage and increase in particle settling velocity. Because τ_{pool} is independent of grain size, the decrease in transport stage with grain size lowers c_b, while the increased settling velocity for large particles lowers L_d, leading to reduced sediment concentrations throughout the plunge pool.

6.4. Influence of Plunge-Pool Radius

The influence of plunge-pool radius on sediment-transport capacity is not as straightforward in our experiments compared to changing Q_w, H_{drop}, and D (Figures 6d and 6e). For experiments with $D = 7$ mm grains, plunge pools with $r_{pool} = 7.7$ cm were completely filled with sediment, even at equilibrium for clear-water discharge, while narrower ($r_{pool} = 5.1$ cm) pools had equilibrium depths which shallowed with increasing sediment supply, all else held constant. This trend is in agreement with our theory where, for a given pool depth, decreasing plunge-pool radius leads to higher sediment-transport capacity, while for a given sediment supply, decreasing plunge-pool radius leads to a deeper equilibrium pool depth (Figure 6d). However, when using finer sediment ($D = 2.4$ mm), plunge pools of different radii had approximately the same equilibrium pool depths (within measurement error) for identical forcing (with the exception of at the largest sediment fluxes when small differences in pool depth emerged), in contrast to our model predictions that, for a given pool depth, sediment-transport capacity should increase with decreasing r_{pool} (Figure 6e).

Increases in plunge-pool radius result in a reduction of Q_{sc_pool} in our model when all other parameters are held constant for two reasons. First, increasing radius causes a decrease in sediment concentration at the plunge-pool lip as there is a longer length scale over which sediment must be transported (e.g., Figure 3). Second, for a constant water discharge and jet diameter, increases in plunge-pool radius reduce w_{up}, thereby enhancing the influence of particle gravitational settling (lowering L_d) and reducing sediment concentrations in the plunge pool.

6.5. Influence of Froude Number

Although not explored experimentally, our model predicts plunge-pool sediment-transport capacity is independent of Fr_n for subcritical flows ($Fr_n < 1$), as flow acceleration toward the waterfall brink results in a constant value of u_{brink} [*Rouse*, 1936, 1937b; *Hager*, 1983; *Lapotre and Lamb*, 2015] for $Fr_n < 1$. For supercritical flows ($Fr_n > 1$), increasing Fr_n gives increasing u_{brink} which raise τ_{pool} (equation (7)), ultimately leading to increases in Q_{sc_pool} when all else is held constant; however, this effect is small compared to the influence of changing water discharge, waterfall drop height, grain size, pool depth, and pool radius examined above. Fr_n may also play an additional role for 2-D waterfalls because of lateral flow convergence [*Lapotre and Lamb*, 2015].

6.6. Comparison to Previous Models and Overall Model Performance

There exist no previously published models capable of predicting waterfall plunge-pool sediment-transport capacity subject to sediment supply from upstream; however, there are multiple theories which predict equilibrium pool depth under clear-water flow. Theoretical models often assume equilibrium clear-water pool depth is set by the threshold of motion for sediment [e.g., *Stein et al*., 1993]. Calculating expected equilibrium clear-water depths by solving for the pool depth where $\tau_{*pool} = \tau_{*c}$ using equations (7a) and (7b) and setting $\tau_{*c} = 0.045$ overpredicts our observed steady-state depths by a factor of ~1.5 to 4 (Figure 7a). Using larger values of τ_{*c} can produce a better prediction. However, the hypothesis that clear-water scour depths are set by τ_{*c} is not supported by our observations of actively mobile bed sediment even when plunge pools reached steady-state depths under clear-water flow. Instead, steady-state pool depths are set by the jet's ability to suspend sediment and transport it up and out of the pool, rather than by the threshold of motion.

Comparing our clear-water results with predictions of steady-state pool depth from the empirical models of *Mason and Arumugam* [1985] and *Pagliara et al*. [2006] produced mixed results with the *Mason and Arumugam* [1985] model underpredicting equilibrium depths by up to a factor of ~2.5 (Figure 7b), while the *Pagliara et al*. [2006] model overpredicts equilibrium depths by up to a factor of ~2 (Figure 7c). This discrepancy may be due to the design of these models to predict scour depth of pools in loose

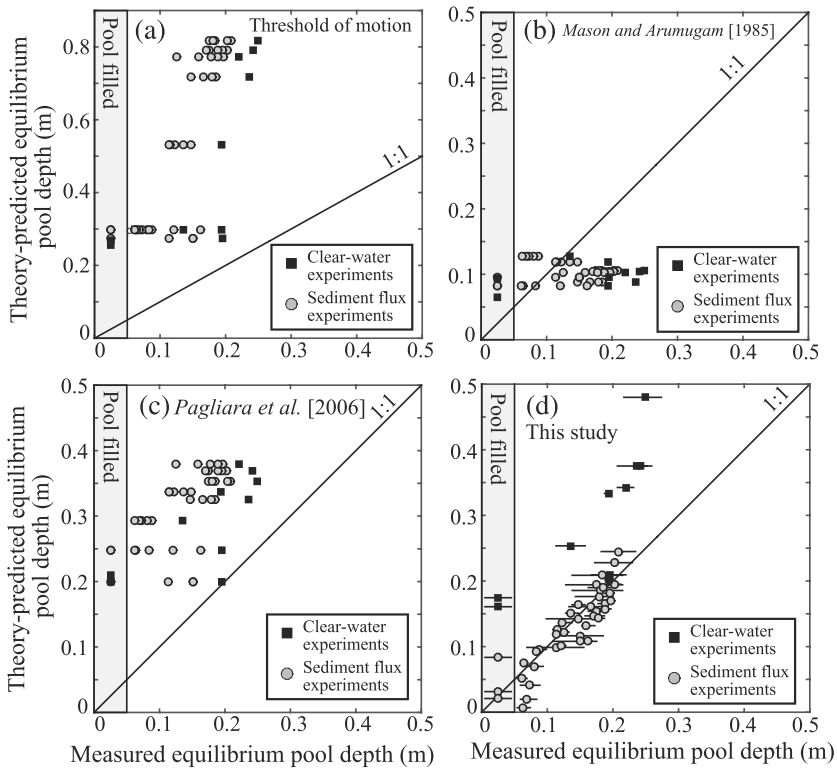

Figure 7. Comparison of pool depth, h_{pool}, measured at equilibrium from our experiments with theory-predicted equilibrium depth using (a) threshold of motion, (b) *Mason and Arumugam* [1985], (c) *Pagliara et al.* [2006], and (d) this study. Error bars in Figure 7d denote topographic variability of pool alluvial floors; identical error bars apply to Figures 7a–7c but were removed for clarity. We calculate tailwater depth above the plunge-pool lip assuming $Fr = 1$ for both the *Pagliara et al.* [2006] and *Mason and Arumugam* [1985] predictions. The *Pagliara et al.* [2006] model also requires an estimate of jet air content which we did not measure in our experiments and set to 0.5. Shaded gray box in all panels marks measured depths less than 5 cm where we observed filled plunge pools with fluidized beds.

sediment with self-formed walls in contrast to our experiments with fixed, vertical walls. Additionally, the *Mason and Arumugam* [1985] model is calibrated using cohesive soils in contrast to the noncohesive sediment in our experiments.

Our model also tends to over predict equilibrium clear-water pool depths by up to a factor ~2 (Figure 7d). For clear-water cases, our model results are sensitive to the choice of reference sediment flux, Q_{*s_pool}, below which we set sediment transport to zero (e.g., $Q_{sc\_pool} = 0$ for $Q_{*s\_pool} < 2 \times 10^{-5}$, section 3.4). Using a larger value of Q_{*s_pool} would result in a better prediction for the clear-water experiments, but at the expense of the goodness of fit with the sediment feed experiments.

Unlike previous models [e.g., *Mason and Arumugam*, 1985; *Stein et al.*, 1993; *Pagliara et al.*, 2006], our new theory explicitly accounts for upstream sediment supply. For the sediment feed experiments, our model agrees with the data for 37 of our 40 measurements within a factor of 1.5, and 17 of 40 measurements match predictions within measurement error ($R^2 = 0.8$ when comparing to the 1:1 line in Figure 7d). Predictions of plunge-pool sediment-transport capacity have increased variability compared to steady-state pool depth predictions due to the nonlinear relationship between Q_{sc_pool} and equilibrium pool depth (Figure 6). As such, our order centimeter-scale measurement error in equilibrium pool depth results in approximately order of magnitude variability in predictions of sediment-transport capacity.

7. Discussion

7.1. Limitations of the Model

Our plunge-pool sediment-transport capacity model has variable success in matching the experimentally observed values of plunge-pool steady-state depth. Misfits might occur due to incorrect parameterizations

of constants within our model (e.g., k_2, C_{f_pool}, and v_e) or due to the lack of inclusion of physical processes within our model framework. We explored the effect of changing the sediment entrainment coefficient, k_2, the coefficient k_1 (which determines the eddy viscosity, v_e), and the plunge-pool friction factor, C_{f_pool}. Increases in k_2, C_{f_pool}, and v_e all lead to predictions of higher sediment-transport capacity or deeper equilibrium pool depths, all else held constant. While changing these coefficients can lead to better predictions for a single experimental set, they cause predictions to worsen for other experimental sets and do not collapse the data overall. This suggests that discrepancies between the model predictions and experimental observations likely come from physical processes present within plunge pools which are not incorporated within our model.

Our experiments (section 6.1) highlight many physical processes that are not included in our simplified theory. For example, as plunge pools transiently aggraded to shallow pool depths ($h_{pool} < \sim 5$ cm), we observed a change in process where the bed became fluidized, likely changing entrainment mechanics and the effective fluid density and viscosity in that region. This process promotes shallower pools than predicted (e.g., Exp 9 and Exp 10, Figure 6d). Similarly, we observed grain-grain interactions within the near-bed active layer and at times between grains suspended in the water column in our experiments (Movie S1). These grain-grain interactions are not accounted for in our model, in which we assume dilute suspension of grains, but could result in significant bed load transport in very shallow pools or yield lower net settling velocities [e.g., *Richardson and Zaki*, 1954] in deeper pools.

Our experimental plunge pools had complex hydraulics where eddies of various scales caused the flow to overturn, sediment transport to occur in pulses, and sediment to concentrate at the downstream pool wall (Figure 5b and Movie S1). These processes may violate our assumptions of axisymmetric flow, a constant eddy viscosity in the vertical and radial directions, and constant w_{up} within the jet return-flow region. While these assumption are necessary to achieve an analytical solution, eddy viscosities are typically parametrized to vary with distance from a boundary in shear flows [e.g., *Prandtl*, 1925; *Rouse*, 1937a], and the upward return flow is likely spatially variable [e.g., *Robinson et al*., 2000; *Bennett and Alonso*, 2005].

Our experiments had a small degree of aeration within the waterfall jet, and the impinging jet further entrained air into the plunge pool (e.g., Figure 5b and Movie S1). Air entrainment in steps and waterfalls is common [e.g., *Valle and Pasternack*, 2006]; however, the relationship between plunge-pool depth and aeration is complicated, and it is unclear how to incorporate aeration into the model at present. For example, experiments have shown jet aeration typically leads to a reduction in equilibrium pool depth [e.g., *Canepa and Hager*, 2003; *Xu et al*., 2004; *Pagliara et al*., 2006], although aeration has also been suggested to more efficiently allow plucking of bedrock blocks which could increase pool depths [*Bollaert*, 2002; *Bollaert and Schleiss*, 2003].

The extent to which the effects missing from our model (i.e., bed fluidization, grain-grain interactions, complex flow hydraulics, and aeration) influence sediment transport may also depend on the particle grain size. For example, large grains with high gravitational settling velocities and small advection lengths may be more sensitive to local flow dynamics than small grains [*Ganti et al*., 2014]. This may be a possible explanation for our experimental observations of sediment-transport capacity being insensitive to plunge-pool radius for $D = 2.4$ mm compared to decreasing sediment-transport capacity with increasing radius for $D = 7$ mm grains (Figures 6d and 6e). If this is correct, replicate experiments with narrower plunge pools and coarse grain sizes may be expected to show no variation in sediment-transport capacity with pool radius, as the larger jet return flow velocity at small pipe diameters could cause particle advection length scales to approach the plunge-pool radius. We attempted experiments like these (not reported); however, experiments with $r_{pool} < 5.2$ cm are difficult as the plunge-pool diameter approaches that of waterfall jet, which violates central assumptions in our model.

7.2. Application to Natural Waterfalls

With the experimentally tested model for plunge-pool sediment transport in hand, we now return to the field cases that motivated this study and were used to define the parameter space explored in the experiments (section 4). Our field surveys allow comparison of measured plunge-pool depths to the expected equilibrium depths from both clear-water theories [e.g., *Pagliara et al*., 2006] and our sediment transport theory. Surveyed plunge pools are ~3–300 times shallower than predicted for clear-water overspill during a 2 year recurrence

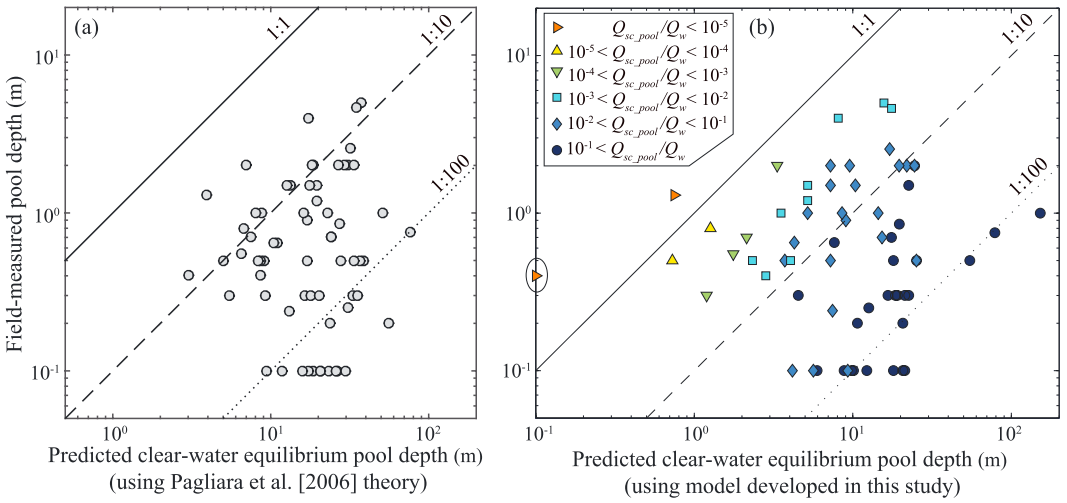

Figure 8. Comparison of field-measured plunge-pool depth (Table S1 and see supporting information S1 for field methods) versus predictions for pool depth (h_{pool}) at equilibrium assuming no sediment supply for 2 year recurrence interval floods using (a) *Pagliara et al.* [2006] and (b) theory developed herein. Points below the 1:1 line represent pools shallower than predicted for clear-water flow. Points in Figure 8b are color-coded by the upstream sediment concentrations (Q_{sc_pool}/Q_w) needed to fit the observed pool depth at steady state, indicating that greater departure from the 1:1 line (i.e., partially alluviated and sediment-filled pools) requires higher sediment concentration from upstream to maintain a steady state depth. The circled point on the *y* axis in Figure 8b is a plunge pool which is predicted to be completely filled with sediment under clear-water discharge. All model calculations used the grain size of sediment measured in the plunge pool. For predictions in Figure 8a, we assumed a jet air content of 0.5.

interval flood using the approach of *Pagliara et al.* [2006] (Figure 8a). *Pagliara et al.* [2006] assume both clear-water discharge and self-formed pool walls, neither of which are likely for natural, bedrock-walled plunge pools. Additionally, most surveyed pools are shallower than predicted at equilibrium under clear-water conditions using our theory (Figure 8b), suggesting that the discrepancy is likely due to sediment supply rather than plunge-pool geometry.

We used our model to calculate the expected steady-state sediment concentration (Q_{sc_pool}/Q_w) for a 2 year recurrence interval flood discharge that is necessary to fit the observed pool depths, assuming that they are at steady state (Figure 8b). Our analysis indicates that the observed pool depths can be explained by upstream sediment concentrations that range from less than a hundredth of a percent to greater than 10% by volume. The theory suggests that the shallower pools, if at equilibrium, are associated with rivers that deliver a greater sediment supply (Figure 8b). However, field measurements of pool depth can be sensitive to the magnitude and duration of clear water scour occurring on the rising and falling limb of hydrographs [*Buffington et al.*, 2002], and may reflect disequilibrium conditions.

7.3. Implications for Habitat, Hazards, and Bedrock Erosion

While waterfall plunge pools typically have small volumes compared to total fluvial sediment flux over the course of a flood (such that storage of sediment in or scour from pools should not largely influence overall sediment budgets), the thickness of sediment fill has implications for habitat availability and natural hazards. Deep, sediment-free or partially-filled pools provide habitat for aquatic organisms [e.g., *Matthews et al.*, 1994; *Magoulick and Kobza*, 2003; *Bond et al.*, 2008] and sediment-filled pools provide conditions to initiate debris flows [e.g., *Griffiths et al.*, 2004; *Larsen et al.*, 2006]. The model developed here provides a first-order tool for land managers to estimate sediment filling and evacuation of waterfall plunge pools in response to changes in river hydraulics or upstream sediment supply. For cases where the upstream sediment supply (Q_s) is known, our plunge-pool sediment-transport capacity model can be used to route sediment through plunge pools and track plunge-pool alluvial filling and evacuation, as sediment should be deposited in pools when $Q_{sc\_pool} < Q_s$, sediment should pass through pools when $Q_{sc\_pool} = Q_s$, and sediment should be scoured from pools when $Q_{sc\_pool} > Q_s$.

Our plunge-pool sediment-transport capacity model also can be coupled with physically based bedrock erosion models [e.g., *Lamb et al.*, 2007] to predict waterfall plunge-pool bedrock abrasion over thousands of years. Over such timescales, cycles of sediment fill and evacuation from waterfall plunge pools should influence bedrock erosion as vertical incision requires exposure of the bedrock floor of the pool, while plunge-pool walls are free to erode even when the bed is covered with sediment. Thus, when $Q_{sc\_pool} > Q_s$, pools can scour to bedrock and vertically incise, whereas when $Q_{sc\_pool} < Q_s$ sediment deposits at the base of the pool, armoring the bed, and preventing vertical incision (but potentially still allowing for lateral erosion), analogous to the role sediment cover plays in controlling bedrock channel width [e.g., *Sklar and Dietrich*, 2004; *Finnegan et al.*, 2007; *Turowski et al.*, 2008].

8. Conclusions

We developed an analytical model to predict the sediment-transport capacity for waterfall plunge pools based on seven field-measurable variables (water discharge, waterfall drop height, plunge-pool depth and radius, grain size, and upstream channel slope and width). The model is designed for bedrock-walled and alluvial-floored pools with cylindrical geometry where the alluvial fill is free to aggrade and degrade. The model predicts that plunge pools self-adjust their depth through erosion and deposition of sediment in response to the imposed sediment supply from upstream. Changes in pool depth, in turn, affect jet hydrodynamics and sediment flux out of the pool, and negative feedbacks exist that drive a pool toward a steady-state depth for a given waterfall geometry, sediment supply, and water discharge. Laboratory experiments largely confirm these predictions and show that, all else equal, plunge-pool sediment-transport capacity increases for shallower pools, greater water discharge, higher waterfall drop height, and smaller grain size. The theory matches most of the experimental data within a factor of ~1.5, and discrepancies may be due to 3-D flow hydraulics, grain-grain interactions, and jet aeration which are not accounted for in the model. Field surveys of 75 waterfall plunge pools show that many natural pools tend to be filled with sediment resulting in pools that are shallower than predicted at equilibrium for a 2 year recurrence flood with no sediment supply, thus suggesting that the upstream sediment supply plays an important role in reducing observed plunge-pool depths. The model presented here provides a framework for future applications including sediment routing, habitat availability, debris flow initiation, and bedrock erosion.

Notation

A_{jet}	waterfall jet area (L^2)
A_{pool}	plunge-pool area (L^2)
C_d	waterfall jet diffusion coefficient (dimensionless)
C_{f_pool}	plunge-pool friction factor (dimensionless)
C_{f_river}	river friction factor (dimensionless)
D	grain diameter (L)
Fr_n	normal Froude number upstream of the waterfall (dimensionless)
H_{drop}	waterfall drop height (L)
L_d	characteristic length scale over which turbulence mixes sediment (L)
Q_s	upstream sediment supply (L/T^3)
Q_{*s_pool}	dimensionless plunge-pool sediment flux (dimensionless)
Q_{sc_pool}	plunge-pool sediment-transport capacity (L/T^3)
Q_w	water discharge (L/T^3)
R	submerged sediment density (dimensionless)
S	channel slope (dimensionless)
W	channel width (L)
a_1	constant used in calculated particle settling velocity (dimensionless)
a_2	constant used in calculated particle settling velocity (dimensionless)
$b(z)$	jet half-width as a function of height above pool floor (L)
c	volumetric sediment concentration (dimensionless)
$\bar{c}$	sediment concentration temporally averaged over turbulence (dimensionless)
c'	turbulent fluctuations in sediment concentration (dimensionless)

c_b	reference near-bed sediment concentration in jet-descending region (dimensionless)
c_o	reference near-bed sediment concentration at (r_{pool}, z_{mixed}) (dimensionless)
g	gravitational acceleration (L/T^2)
h_n	normal flow depth upstream of the waterfall (L)
h_{pool}	plunge-pool depth (L)
k_1	coefficient in estimating eddy diffusivity (dimensionless)
k_2	constant in sediment entrainment formula (dimensionless)
r	radial coordinate (L)
r_{jet}	waterfall jet radius at point of impact with water surface (L)
r_{pool}	plunge-pool radius (L)
t	time (T)
u_{*pool}	shear velocity at the plunge-pool bed (L/T)
u_{brink}	water velocity at the waterfall brink (L/T)
u_{impact}	jet velocity upon impact with the plunge-pool floor (L/T)
u_{jet}	jet velocity upon impact with the plunge-pool water surface (L/T)
u_{lip}	water velocity at the downstream plunge-pool lip (L/T)
u_n	normal water velocity upstream of the waterfall (L/T)
u_r	radial water velocity (L/T)
u_r'	turbulent fluctuations in radial water velocity (L/T)
u_θ	azimuthal water velocity (L/T)
w_{net}	net particle settling velocity (L/T)
w_s	particle gravitational settling velocity (L/T)
w_{up}	vertical velocity of the jet return flow (L/T)
w_{up}'	turbulent fluctuations in vertical velocity of the jet return flow (L/T)
z	vertical coordinate (L)
z_{BR}	elevation of the plunge-pool bedrock floor (L)
z_{lip}	elevation of the downstream plunge-pool lip (L)
z_{mixed}	elevation of the top of well-mixed layer near the plunge-pool floor (L)
z_{sed}	elevation of the plunge-pool alluvial floor (L)
z_{water}	elevation of the plunge-pool water surface (L)
z_λ	elevation of the boundary between the ZOEF and ZOFE (L)
β	angle of waterfall jet impact (rad)
γ	virtual origin in estimation of jet half-width (L)
δ	radial distance which sets boundary between descending-flow and jet return-flow regions, equal to twice the jet half-width measured at the pool alluvial floor (L)
θ	azimuthal coordinate (L)
λ	length of ZOFE (L)
ν	kinematic water viscosity (L^2/T)
ν_e	eddy diffusivity (L^2/T)
ρ	fluid density (M/L^3)
ρ_s	sediment density (M/L^3)
τ_{pool}	plunge-pool bed shear stress (M L^{-1} T^{-2})
τ_{river}	river bed shear stress (M L^{-1} T^{-2})
τ_{*c}	critical Shields stress for grain motion (dimensionless)
τ_{*pool}	plunge-pool bed Shields stress (dimensionless)

Acknowledgments

Data presented in this paper, as well as a MATLAB code to calculate plunge-pool sediment-transport capacity, are available in the supporting information or by contacting J.S.S. We are grateful to Brian Fuller for assistance with laboratory experiments and benefitted from conversations with Jeff Prancevic, Andy Thompson, Patrick Sanan, Mike Gurnis, and Jeremy Venditti. Roman DiBiase and Chris Brennen assisted with waterfall surveys and, together with Kelin Whipple, kindly shared photographs and data from plunge pools in the San Gabriel Mountains. Greg Pasternack, two anonymous reviewers, Associate Editor Peter Ashmore, and Editor John Buffington provided constructive comments which improved the structure and presentation of this manuscript. We thank Mike Oxford and the U.S. Forest Service for access to the San Dimas Experimental Forest. We acknowledge funding from NSF (EAR-1147381) and NASA (12PGG120107) to M.P.L and a NSF Graduate Research Fellowship to J.S.S.

References

Abramovich, G., and L. Schindel (1963), *The Theory of Turbulent Jets*, pp. 671, MIT Press, Cambridge, Mass.

Albertson, M. L., Y. B. Dai, R. A. Jensen, and H. Rouse (1950), Diffusion of submerged jets, *Trans. Am. Soc. Civ. Eng.*, *115*, 639–664.

Alonso, C. V., S. J. Bennett, and O. R. Stein (2002), Predicting head cut erosion and migration in concentrated flows typical of upland areas, *Water Resour. Res.*, *38*(12, 1303), doi:10.1029/2001WR001173.

Beltaos, S. (1976), Oblique impingement of plane turbulent jets, *J. Hydraul. Div. ASCE*, *102*(9), 1177–1192.

Beltaos, S., and N. Rajaratnam (1973), Plane turbulent impinging jets, *J. Hydraul. Res.*, *11*(1), 29–59, doi:10.1080/00221687309499789.

Bennett, S. J., and C. V. Alonso (2005), Kinematics of flow within headcut scour holes on hillslopes, *Water Resour. Res.*, *41*, W09418, doi:10.1029/2004WR003752.

Bennett, S. J., C. V. Alonso, S. N. Prasad, and M. J. M. Romkens (2000), Experiments on headcut growth and migration in concentrated flows typical of upland areas, *Water Resour. Res.*, *36*(7), 1911–1922, doi:10.1029/2000WR900067.
Berlin, M. M., and R. S. Anderson (2007), Modeling of knickpoint retreat on the Roan Plateau, western Colorado, *J. Geophys. Res.*, *112*, F03S06, doi:10.1029/2006JF000553.
Bollaert, E. (2002), The influence of plunge pool air entrainment on the presence of free air in rock joints, in *Rock Scour Due To Falling High-Velocity Jets*, edited by A. Schleiss and E. Bollaert, A A. Balkema Publishers, Lisse, Netherlands.
Bollaert, E., and A. Schleiss (2003), Scour of rock due to the impact of plunging high velocity jets. Part I: A state-of-the-art review, *J. Hydraul. Res.*, *41*(5), 451–464, doi:10.1080/00221680309499991.
Bond, N. R., P. S. Lake, and A. H. Arthington (2008), The impacts of drought on freshwater ecosystems: An Australian perspective, *Hydrobiologia*, *600*, 3–16, doi:10.1007/s10750-008-9326-z.
Boulton, A. J. (2003), Parallels and contrasts in the effects of drought on stream macroinvertebrate assemblages, *Freshwater Biol.*, *48*(7), 1173–1185, doi:10.1046/j.1365-2427.2003.01084.x.
Bradbury, L. J. (1965), Structure of a self-preserving turbulent plane jet, *J. Fluid Mech.*, *23*, 31–64, doi:10.1017/s0022112065001222.
Brownlie, W. R. (1981), *Prediction of Flow Depth and Sediment Discharge in Open Channels*, W M. Keck Laboratory of Hydraulics and Water Resources, Pasadena, Calif.
Buffington, J. M., and D. R. Montgomery (1997), A systematic analysis of eight decades of incipient motion studies, with special reference to gravel-bedded rivers, *Water Resour. Res.*, *33*(8), 1993–2029, doi:10.1029/96WR03190.
Buffington, J. M., T. E. Lisle, R. D. Woodsmith, and S. Hilton (2002), Controls on the size and occurrence of pools in coarse-grained forest rivers, *River Res. Appl.*, *18*, 507–531, doi:10.1002/rra.693.
Canepa, S., and W. H. Hager (2003), Effect of jet air content on plunge pool scour, *J. Hydraul. Eng. ASCE*, *129*(5), 358–365, doi:10.1061/(Asce)0733-9429(2003)129:5(358).
Chatanantavet, P., and G. Parker (2006), Modeling the bedrock river evolution of western Kaua'i, Hawai'i, by a physically-based incision model based on abrasion, in *River, Coastal and Estuarine Morphodynamics 2005*, edited by G. Parker and M. Garcia, Taylor and Francis Group, London.
Chow, V. T. (2009), *Open-Channel Hydraulics*, The Blackburn Press, Caldwell, N. J..
Crosby, B. T., and K. X. Whipple (2006), Knickpoint initiation and distribution within fluvial networks: 236 waterfalls in the Waipaoa River, North Island, New Zealand, *Geomorphology*, *82*(1–2), 16–38, doi:10.1016/j.geomorph.2005.08.023.
Crosby, B. T., K. X. Whipple, N. M. Gasparini, and C. W. Wobus (2007), Formation of fluvial hanging valleys: Theory and simulation, *J. Geophys. Res.*, *112*, F03S10, doi:10.1029/2006JF000566.
DiBiase, R. A., K. X. Whipple, A. M. Heimsath, and W. B. Ouimet (2010), Landscape form and millennial erosion rates in the San Gabriel Mountains, CA, *Earth Planet. Sci. Lett.*, *289*(1–2), 134–144, doi:10.1016/j.epsl.2009.10.036.
DiBiase, R. A., K. X. Whipple, M. P. Lamb, and A. M. Heimsath (2015), The role of waterfalls and knickzones in controlling the style and pace of landscape adjustment in the western San Gabriel Mountains, California, *Geol. Soc. Am. Bull.*, *127*(3–4), 539–559, doi:10.1130/B31113.1.
Dietrich, W. E., D. Bellugi, A. M. Heimsath, J. J. Roering, L. Sklar, and J. D. Stock (2003), *Geomorphic Transport Laws for Predicting the Form and Evolution of Landscapes*, *Geophys. Monogr. Ser.*, edited by P. R. Wilcock and R. M. Iverson, pp. 103–132, AGU, Washington D. C., doi:10.1029/GM135.
Ervine, D. A., H. T. Falvey, and W. Withers (1997), Pressure fluctuations on plunge pool floors, *J. Hydraul. Res.*, *35*(2), 257–279, doi:10.1080/00221689709498430.
Ferguson, R. I., and M. Church (2004), A simple universal equation for grain settling velocity, *J. Sediment. Res.*, *74*(6), 933–937, doi:10.1306/051204740933.
Fernandez Luque, R., and R. van Beek (1976), Erosion and transport of bed-load sediment, *J. Hydraul. Res.*, *14*, 127–144, doi:10.1080/00221687609499677.
Ferrier, K. L., J. T. Perron, S. Mukhopadhyay, M. Rosener, J. D. Stock, K. L. Huppert, and M. Slosberg (2013), Covariation of climate and long-term erosion rates across a steep rainfall gradient on the Hawaiian island of Kaua'i, *Geol. Soc. Am. Bull.*, *125*(7–8), 1146–1163, doi:10.1130/B30726.1.
Finnegan, N. J., L. S. Sklar, and T. K. Fuller (2007), Interplay of sediment supply, river incision, and channel morphology revealed by the transient evolution of an experimental bedrock channel, *J. Geophys. Res.*, *112*, F03S11, doi:10.1029/2006JF000569.
Fiorotto, V., and A. Rinaldo (1992), Fluctuating uplift and lining design in spillway stilling basins, *J. Hydraul. Eng. ASCE*, *118*(4), 578–596, doi:10.1061/(Asce)0733-9429(1992)118:4(578).
Flores-Cervantes, J. H., E. Istanbulluoglu, and R. L. Bras (2006), Development of gullies on the landscape: A model of headcut retreat resulting from plunge pool erosion, *J. Geophys. Res.*, *111*, F01010, doi:10.1029/2004JF000226.
Ganti, V., M. P. Lamb, and B. A. McElroy (2014), Quantitative bounds on morphodynamics and implications for reading the sedimentary record, *Nat. Commun.*, *5*, doi:10.1038/ncomms4298.
Garcia, M. H. (2008), Sediment transport and morphodynamics, in *Sedimentation Engineering: Processes, Measurements, Modeling, and Practice*, edited by M. H. Garcia, American Society of Civ. Engineers, Reston, Va., doi:10.1061/9780784408148.
Garcia, M. H., and G. Parker (1991), Entrainment of bed sediment into suspension, *J. Hydraul. Eng. ASCE*, *117*(4), 414–435, doi:10.1061/(Asce)0733-9429(1991)117:4(414).
Gaudio, R., and A. Marion (2003), Time evolution of scouring downstream of bed sills, *J. Hydraul. Res.*, *41*(3), 271–284.
Ghaneeizad, S. M., J. F. Atkinson, and S. J. Bennett (2015), Effect of flow confinement on the hydrodynamics of circular impinging jets: Implications for erosion assessment, *Environ. Fluid Mech.*, *15*(1), 1–25, doi:10.1007/s10652-014-9354-3.
Giger, M., T. Dracos, and G. H. Jirka (1991), Entrainment and mixing in plane turbulent jets in shallow-water, *J. Hydraul. Res.*, *29*(5), 615–642, doi:10.1080/00221689109498980.
Gilbert, G. K. (1890), The history of the Niagara River, extracted from the sixth annual report to the commissioners of the state reservation at Niagara, Albany, NY.
Gilbert, G. K. (1907), The rate of recession of Niagara Falls, *U.S. Geol. Surv. Bull.*, *306*, 1–31.
Godt, J. W., and J. A. Coe (2007), Alpine debris flows triggered by a 28 July 1999 thunderstorm in the central Front Range, Colorado, *Geomorphology*, *84*(1–2), 80–97, doi:10.1016/j.geomorph.2006.07.009.
Griffiths, P. G., R. H. Webb, and T. S. Melis (2004), Frequency and initiation of debris flows in Grand Canyon, Arizona, *J. Geophys. Res.*, *109*, F04002, doi:10.1029/2003JF000077.
Hager, W. H. (1983), Hydraulics of plane free overfall, *J. Hydraul. Eng. ASCE*, *109*(12), 1683–1697, doi:10.1061/(ASCE)0733-9429(1983)109:12(1683).
Hanson, G. J., K. M. Robinson, and K. R. Cook (2002), Scour below an overfall: Part II. Prediction, *Trans. ASAE*, *45*(4), 957–964.
Haviv, I., Y. Enzel, K. X. Whipple, E. Zilberman, A. Matmon, J. Stone, and K. L. Fifield (2010), Evolution of vertical knickpoints (waterfalls) with resistant caprock: Insights from numerical modeling, *J. Geophys. Res.*, *115*, F03028, doi:10.1029/2008JF001187.

Hawkins, C. P., et al. (1993), A hierarchical approach to classifying stream habitat features, *Fisheries*, *18*(6), 3–12, doi:10.1577/1548-8446(1993)018<0003:ahatcs>2.0.co;2.
Holland, W. N., and G. Pickup (1976), Flume study of knickpoint development in stratified sediment, *Geol. Soc. Am. Bull.*, *87*(1), 76–82, doi:10.1130/0016-7606(1976)87<76:fsokdi>2.0.co;2.
Howard, A. D., W. E. Dietrich, and M. A. Seidl (1994), Modeling fluvial erosion on regional to continental scales, *J. Geophys. Res.*, *99*(B7), 13,971–13,986, doi:10.1029/94JB00744.
Lake, P. S. (2003), Ecological effects of perturbation by drought in flowing waters, *Freshwater Biol.*, *48*(7), 1161–1172, doi:10.1046/j.1365-2427.2003.01086.x.
Lamb, M. P., and W. E. Dietrich (2009), The persistence of waterfalls in fractured rock, *Geol. Soc. Am. Bull.*, *121*(7–8), 1123–1134, doi:10.1130/b26482.1.
Lamb, M. P., A. D. Howard, W. E. Dietrich, and J. T. Perron (2007), Formation of amphitheater-headed valleys by waterfall erosion after large-scale slumping on Hawai'i, *Geol. Soc. Am. Bull.*, *119*(7–8), 805–822, doi:10.1130/b25986.1.
Lamb, M. P., J. S. Scheingross, W. H. Amidon, E. Swanson, and A. Limaye (2011), A model for fire-induced sediment yield by dry ravel in steep landscapes, *J. Geophys. Res.*, *116*, F03006, doi:10.1029/2010JF001878.
Lamb, M. P., N. J. Finnegan, J. S. Scheingross, and L. S. Sklar (2015), New insights into the mechanics of fluvial bedrock erosion through flume experiments and theory, *Geomorphology*, *244*, 33–55, doi:10.1016/j.geomorph.2015.03.003.
Lane, E. W. (1955), The importance of fluvial morphology in hydraulic engineering, *Proc. Am. Soc. Civ. Eng.*, *81*(745), 1–17.
Lapotre, M. G. A., and M. P. Lamb (2015), Hydraulics of floods upstream of horseshoe canyons and waterfalls, *J. Geophys. Res. Earth Surf.*, *120*, 1227–1250, doi:10.1002/2014JF003412.
Larsen, I. J., J. L. Pederson, and J. C. Schmidt (2006), Geologic versus wildfire controls on hillslope processes and debris flow initiation in the Green River canyons of Dinosaur National Monument, *Geomorphology*, *81*(1–2), 114–127, doi:10.1016/j.geomorph.2006.04.002.
Lenzi, M. A., and F. Comiti (2003), Local scouring and morphological adjustments in steep channels with check-dam sequences, *Geomorphology*, *55*(1–4), 97–109, doi:10.1016/S0169-555x(03)00134-X.
Lenzi, M. A., A. Marion, F. Comiti, and R. Gaudio (2002), Local scouring in low and high gradient streams at bed sills, *J. Hydraul. Res.*, *40*(6), 731–739.
Lenzi, M. A., A. Marion, and F. Comiti (2003), Local scouring at grade-control structures in alluvial mountain rivers, *Water Resour. Res.*, *39*(7), 1176, doi:10.1029/2002WR001815.
Lisle, T. E. (1987), Using residual depths to monitor pool depths independently from discharge, USDA Forest Service Research Note PSW-394, Pacific Southwest Research Station, Albany, Calif.
Lisle, T. E., and S. Hilton (1992), The volume of fine sediment in pools: An index of sediment supply in gravel-bed streams, *Water Resour. Bull.*, *28*(2), 371–383.
Mackey, B. H., J. S. Scheingross, M. P. Lamb, and K. A. Farley (2014), Knickpoint formation, rapid propagation, and landscape response following coastal cliff retreat at the last interglacial sea-level highstand: Kaua'i, Hawai'i, *Geol. Soc. Am. Bull.*, *126*(7–8), 925–942, doi:10.1130/b30930.1.
Mackin, J. H. (1948), Concept of the graded river, *Geol. Soc. Am. Bull.*, *59*(5), 463–511, doi:10.1130/0016-7606(1948)59[463:COTGR]2.0.CO;2.
Magoulick, D. D., and R. M. Kobza (2003), The role of refugia for fishes during drought: A review and synthesis, *Freshwater Biol.*, *48*(7), 1186–1198, doi:10.1046/j.1365-2427.2003.01089.x.
Marion, A., M. A. Lenzi, and F. Comiti (2004), Effect of sill spacing and sediment size grading on scouring at grade-control structures, *Earth Surf. Processes Landforms*, *29*(8), 983–993, doi:10.1002/esp.1081.
Marion, A., M. Tregnaghi, and S. Tait (2006), Sediment supply and local scouring at bed sills in high-gradient streams, *Water Resour. Res.*, *42*, W06416, doi:10.1029/2005WR004124.
Mason, P. J., and K. Arumugam (1985), Free jet scour below dams and flip buckets, *J. Hydraul. Eng. ASCE*, *111*(2), 220–235, doi:10.1061/(ASCE)0733-9429(1985)111:2(220).
Matthews, K. R., N. H. Berg, D. L. Azuma, and T. R. Lambert (1994), Cool water formation and trout habitat use in a deep pool in the Sierra-Nevada, California, *Trans. Am. Fish. Soc.*, *123*(4), 549–564, doi:10.1577/1548-8659(1994)123<0549:cwfath>2.3.co;2.
McLean, S. R. (1992), On the calculation of suspended-load for noncohesive sediments, *J. Geophys. Res.*, *97*(C4), 5759–5770, doi:10.1029/91JC02933.
Meyer-Peter, E., and R. Mueller (1948), Formulas for bedload transport, paper presented at Proceedings of the 2nd Congress, IAHR, Stockholm.
Nezu, L., and H. Nakagawa (1993), *Turbulence in Open Channel Flows*, pp. 281, Rotterdam, Netherlands.
Nielsen, J. L., T. E. Lisle, and V. Ozaki (1994), Thermally stratified pools and their use by Steelhead in northern California Streams, *Trans. Am. Fish. Soc.*, *123*(4), 613–626, doi:10.1577/1548-8659(1994)123<0613:tspatu>2.3.co;2.
Nitsche, M., D. Rickenmann, J. M. Turowski, A. Badoux, and J. W. Kirchner (2011), Evaluation of bedload transport predictions using flow resistance equations to account for macro-roughness in steep mountain streams, *Water Resour. Res.*, *47*, W08513, doi:10.1029/2011WR010645.
Pagliara, S., W. H. Hager, and H. E. Minor (2006), Hydraulics of plane plunge pool scour, *J. Hydraul. Eng. ASCE*, *132*(5), 450–461, doi:10.1061/(asce)0733-9429(2006)132:5(450).
Pagliara, S., M. Amidei, and W. H. Hager (2008a), Hydraulics of 3D plunge pool scour, *J. Hydraul. Eng. ASCE*, *134*(9), 1275–1284, doi:10.1061/(Asce)0733-9429(2008)134:9(1275).
Pagliara, S., W. H. Hager, and J. Unger (2008b), Temporal evolution of plunge pool scour, *J. Hydraul. Eng. ASCE*, *134*(11), 1630–1638, doi:10.1061/(Asce)0733-9429(2008)34:11(1630).
Pagliara, S., D. Roy, and M. Palermo (2010), 3D plunge pool scour with protection measures, *J. Hydro Environ. Res.*, *4*(3), 225–233, doi:10.1016/j.jher.2009.10.014.
Pagliara, S., M. Palermo, and I. Carnacina (2011), Expanding pools morphology in live-bed conditions, *Acta Geophys.*, *59*(2), 296–316, doi:10.2478/s11600-010-0048-z.
Pagliara, S., M. Palermo, and I. Carnacina (2012a), Live-bed scour downstream of block ramps for low densimetric Froude numbers, *Int. J. Sediment Res.*, *27*(3), 337–350.
Pagliara, S., M. Palermo, and D. Roy (2012b), Stilling basin erosion due to vertical crossing jets, *J. Hydraul. Res.*, *50*(3), 290–297, doi:10.1080/00221686.2012.669534.
Parker, G. (1991), Selective sorting and abrasion of river gravel. 2. Applications, *J. Hydraul. Eng. ASCE*, *117*(2), 150–171, doi:10.1061/(Asce)0733-9429(1991)117:2(150).
Parker, G. (2008), Transport of gravel and sediment mixtures, in *Sedimentation Engineering: Processes, Measurements, Modeling, and Practice*, edited by M. H. Garcia, American Society of Civ. Engineers, Reston, Va., doi:10.1061/9780784408148.

Parker, G., P. C. Klingeman, and D. G. McLean (1982), Bedload and size distribution in paved gravel-bed streams, *J. Hydraul. Eng. ASCE*, *108*(4), 544–571.
Pasternack, G. B., C. R. Ellis, and J. D. Marr (2007), Jet and hydraulic jump near-bed stresses below a horseshoe waterfall, *Water Resour. Res.*, *43*, W07449, doi:10.1029/2006WR005774.
Pizzuto, J. E. (1987), Sediment diffusion during overbank flows, *Sedimentology*, *34*(2), 301–317, doi:10.1111/j.1365-3091.1987.tb00779.x.
Prancevic, J. P., M. P. Lamb, and B. M. Fuller (2014), Incipient sediment motion across the river to debris-flow transition, *Geology*, *42*(3), 191–194, doi:10.1130/g34927.1.
Prandtl, L. (1925), A report on testing for built-up turbulence, *Z. Angew. Math. Mech.*, *5*, 136–139.
Rajaratnam, N. (1976), *Turbulent Jets*, Elsevier, Amsterdam.
Recking, A. (2009), Theoretical development on the effects of changing flow hydraulics on incipient bed load motion, *Water Resour. Res.*, *45*, W04401, doi:10.1029/2008WR006826.
Rempel, L. L., J. S. Richardson, and M. C. Healey (1999), Flow refugia for benthic macroinvertebrates during flooding of a large river, *J. N. Am. Benthol. Soc.*, *18*(1), 34–48, doi:10.2307/1468007.
Richardson, J., and W. Zaki (1954), Sedimentation and fluidisation: Part I, *Trans. Inst. Chem. Eng.*, *32*, 35–53.
Robinson, K. M., K. R. Cook, and G. J. Hanson (2000), Velocity field measurements at an overfall, *Trans. ASAE*, *43*(3), 665–670.
Rouse, H. R. (1936), Discharge characteristics of the free overfall, *Civ. Eng.*, *6*, 257–260.
Rouse, H. R. (1937a), Modern conceptions of the mechanics of turbulence, *Trans. Am. Soc. Civ. Eng.*, *102*(1), 463–543.
Rouse, H. R. (1937b), Pressure distribution and acceleration at the free overfall, *Civ. Eng.*, *7*, 518.
Rowland, J. C., M. T. Stacey, and W. E. Dietrich (2009), Turbulent characteristics of a shallow wall-bounded plane jet: Experimental implications for river mouth hydrodynamics, *J. Fluid Mech.*, *627*, 423–449, doi:10.1017/s0022112009006107.
Sklar, L. S., and W. E. Dietrich (2004), A mechanistic model for river incision into bedrock by saltating bed load, *Water Resour. Res.*, *40*, doi:10.1029/2003WR002496.
Stein, O. R., and P. Y. Julien (1993), Criterion delineating the mode of headcut migration, *J. Hydraul. Eng. ASCE*, *119*(1), 37–50, doi:10.1061/(asce)0733-9429(1993)119:1(37).
Stein, O. R., C. V. Alonso, and P. Y. Julien (1993), Mechanics of jet scour downstream of a headcut, *J. Hydraul. Res.*, *31*(6), 723–738, doi:10.1080/00221689309498814.
Stock, G. M., R. S. Anderson, and R. C. Finkel (2005), Rates of erosion and topographic evolution of the Sierra Nevada, California, inferred from cosmogenic Al-26 and Be-10 concentrations, *Earth Surf. Processes Landforms*, *30*(8), 985–1006, doi:10.1002/esp.1258.
Tinker, K., and E. Wohl (1998), A primer on bedrock channels, in *Rivers Over Rock: Fluvial Processes in Bedrock Channels*, *AGU Geophys. Monogr.*, vol. 107, edited by K. Tinker and E. Wohl, AGU, Washington, D. C.
Torgersen, C. E., D. M. Price, H. W. Li, and B. A. McIntosh (1999), Multiscale thermal refugia and stream habitat associations of chinook salmon in northeastern Oregon, *Ecol. Appl.*, *9*(1), 301–319, doi:10.2307/2641187.
Tregnaghi, M., A. Marion, A. Bottacin-Busolin, and S. J. Tait (2011), Modelling time varying scouring at bed sills, *Earth Surf. Processes Landforms*, *36*(13), 1761–1769, doi:10.1002/esp.2198.
Turowski, J. M., N. Hovius, M.-L. Hsieh, D. Lague, and M.-C. Chen (2008), Distribution of erosion across bedrock channels, *Earth Surf. Processes Landforms*, *33*(3), 353–363, doi:10.1002/esp.1559.
Valle, B. L., and G. B. Pasternack (2006), Air concentrations of submerged and unsubmerged hydraulic jumps in a bedrock step-pool channel, *J. Geophys. Res.*, *111*, F03016, doi:10.1029/2004JF000140.
van Rijn, L. C. (1984), Sediment transport. Part II: Suspended load transport, *J. Hydraul. Eng.*, *110*, 1613–1641, doi:10.1061/(ASCE)0733-9429(1984)110:11(1613).
Weissel, J. K., and M. A. Seidl (1997), Influence of rock strength properties on escarpment retreat across passive continental margins, *Geology*, *25*(7), 631–634, doi:10.1130/0091-7613(1997)025<0631:iorspo>2.3.co;2.
Wells, R. R., S. J. Bennett, and C. V. Alonso (2010), Modulation of headcut soil erosion in rills due to upstream sediment loads, *Water Resour. Res.*, *46*, W12531, doi:10.1029/2010WR009433.
Xu, W. L., H. S. Liao, Y. Q. Yang, and C. G. Wu (2002), Turbulent flow and energy dissipation in plunge pool of high arch dam, *J. Hydraul. Res.*, *40*(4), 471–476, doi:10.1080/00221680209499889.
Xu, W. L., J. Deng, J. X. Qu, S. J. Liu, and W. Wang (2004), Experimental investigation on influence of aeration on plane jet scour, *J. Hydraul. Eng. ASCE*, *130*(2), 160–164, doi:10.1061/(Asce)0733-9429(2004)130:2(160).
Yager, E. M., J. W. Kirchner, and W. E. Dietrich (2007), Calculating bed load transport in steep boulder bed channels, *Water Resour. Res.*, *43*, W07418, doi:10.1029/2006WR005432.
Yager, E. M., W. E. Dietrich, J. W. Kirchner, and B. W. McArdell (2012), Prediction of sediment transport in step-pool channels, *Water Resour. Res.*, *48*, W01541, doi:10.1029/2011WR010829.
Young, R. (1985), Waterfalls: Form and process, *Z. Geomorphol. Suppl.*, *55*, 81–95.
Zimmermann, A., M. Church, and M. A. Hassan (2010), Step-pool stability: Testing the jammed state hypothesis, *J. Geophys. Res.*, *115*, F02008, doi:10.1029/2009JF001365.